DOKUZ EYLÜL UNIVERSITY

GRADUATE SCHOOL OF NATURAL AND APPLIED SCIENCES

MAPPING OF MAGNETIC FLUX BY USING A CARTESIAN ROBOT

by

Ufuk AKOĞUZ

October, 2019

İZMİR

MAPPING OF MAGNETIC FLUX BY USING A CARTESIAN ROBOT

A Thesis Submitted to the
Graduate School of Natural and Applied Sciences of Dokuz Eylül University
In Partial Fulfillment of the Requirements for the Degree of Master of Science in Mechatronics Engineering

by
Ufuk AKOĞUZ

October, 2019
İZMİR

M. Sc THESIS EXAMINATION RESULT FORM

We have read the thesis entitled **"MAPPING OF MAGNETIC FLUX BY USING A CARTESIAN ROBOT"** completed by **UFUK AKOĞUZ** under supervision of **PROF. HİRA KARAGÜLLE** and we certify that in our opinion it is fully adequate, in scope and in quality, as a thesis for the degree of Master of Science.

Prof. Dr. Hira KARAGÜLLE

Supervisor

Dr. Öğr. Üyesi Şahin Yavuz	Doç. Dr. Levent Çetin
(Jury Member)	(Jury Member)

Prof.Dr. Kadriye ERTEKİN

Director

Graduate School of Natural and Applied Sciences

ACKNOWLEDGEMENTS

First and foremost, I am extremely grateful to my mother for her love, prayers, caring and sacrifices for educating and preparing me for my future. I am very grateful to Prof. Dr. Hira KARAGÜLLE and his assistants for her mentorship, to motivation and material support, and patience he has shown me.

In addition, I would like to thank Bayram BAYRAKTAR for his financial support, Sinan PÖĞÜN for moral and resource support and Yiğit ÇAM for supporting of my continuous improvement.

Ufuk AKOĞUZ

MAPPING OF MAGNETIC FLUX BY USING A CARTESIAN ROBOT

ABSTRACT

The permanent magnet circuits is becoming increasingly important to produce. The general purpose is to separate the ferromagnetic parts in the intended bulk (garbage, wheat, etc.). However, there is no standardized control in their production. However, the magnets coming from the manufacturers those can show variability in attraction forces. This situation becomes important when large and sensitive magnet circuits are made. The control of the magnet circuit to make the intended performance is very important. These magnet circuits are used to protect very expensive devices in the mining and recycling sector. Failure or unplanned maintenance of these devices may results very high costs. Here we have worked on a Cartesian robot with features similar to the CMM to give this control.

In this study, a CAD model of system has been developed and analyzed in Solidworks. The chassis of Cartesian Magnetic Flux Mapper (CMFM) has been assembled from laser cut and on the shelf part.

Keywords: Cartesian robots, magnetic flux mapper, testing and reporting, flaw capturing

KARTEZYEN ROBOT KULLANARAK MANYETİK AKININ HARİTALANDIRILMASI

ÖZ

Kalıcı mıknatıs devrelerinin üretimi giderek daha fazla önem kazanmaktadır. Genel amaçları ferromanyetik parçaları yığın içinden (çöp, buğday vb.) ayırmaktır. Ancak, üretimlerinde standart bir kontrol yoktur. Ancak, üreticilerden gelen mıknatısları çekim kuvvetlerinde değişkenlik görülmektedir. Büyük ve hassas mıknatıs devreleri yapıldığında bu durum önemli hale gelir. Mıknatıs devresinin amacılanan performansa ulaşmasının kontrolü oldukça önemlidir.Bu mıknatıs devreleri madencilik ve geri dönüşüm sektöründe çok pahalı cihazları korumak için kullanılır. Bu cihazların bozulması veya planlamaya bir bakıma girmesi çok yüksek maliyetlere yol açabilir. Bu kontrolü sağlamak için CMM'ye benzer özelliklere sahip bir Kartezyen robot üzerinde çalışıldı.

Bu çalışmada, Solidworks'te bir CAD sistemi modeli geliştirilmiş ve analiz edilmiştir. Kartezyen Manyetik Akı Eşleyici (KMAE) şasesi, lazer kesiminden ve raf bölümünden birleştirildi.

Anahtar Kelimeler: Kartezyen robotlar, manyetik akı haritalandırıcı, test etme ve raporlama, hata yakalama

CONTENTS

Page

LIST OF FIGURES

Page

LIST OF TABLES

Page

CHAPTER ONE

INTRODUCTION

Magnetic Circuit (MCs) are commonly used in Magnetic Separators (MSs). MSs have wide range of uses in many industrial applications such as Recycling, Food Processing, Construction, Casting, etc (Svobodaa & Fujita,2003). MS branches two man branches, those are Permanent Magnetic Separators (PMSs) and Electromagnetic Separators (ESs). In this study chassis of Magnetic Flux Mapper (MFM) for use of quality control and measure of PMS is studied.

When designing or building of MC those are inside of MSs, MCs are designed to achieve to Force Index (FI) at the desired distance to attract ferrous object to separate from bulk. Any failure on manufacturing MC will affect FI thus brings failure on separation process. This kind of separators also used for protection of high value recycling machines such as shredders, granule extruder etc. In such cases, performance confirmation of MCs becomes even more important.

In this study, a way of quality control of MC is studied. As quality control metrics; broken magnet detection, magnetic flux mapping, FI mapping, and digital output reporting have been identified and this study has been tried to reach these results.

In general, the design was inspired by "Coordinate Measuring Machine (CMM)" and 3D printers. The main purpose is to transport the Hall Effect sensor to the desired coordinates precisely with a light construction. In order to lighten the construction, inertial forces must be reduced. This is done by reducing the moving masses and moving them with an appropriate speed profile.

First, "AH49H" was selected as the sensor. This sensor provides a linear measurement from -3000 gauss to 3000 gausses. It is suitable for working with permanent magnets in this work. Because Neodymium (NdFeB) magnets are the most powerful permanent magnets obtained with today's technology. The magnetic flux of 2500-3000 gauss can be obtained on the surface of these magnets. In order to control the movement of the robot, the controller boards are selected as RepRap 1.4 and Arduino Mega that is compatible with RepRap 1.4. This board is commonly used in 3D printer applications. The 5-axis stepper motor is timed and has inputs for various analog and digital sensors. Since the detailed researches were carried out in 3D printers, sigma profiles, laser cutting parts and "on the shelf" bearing products were preferred. Since the basic structure of MCs was rectangular, the axes of motion were decided by Cartesian approach. This makes mapping easier to visualize. To minimize inertia forces The CoreXY method has been used on most moving x and y axis. Thanks to this method, end effector movement is provided without moving the motors. To code the electronics Arduino IDE has been used. And to visualize the data which gathered from Hall Effect sensor and coordinate gather from CMFM Python Programming Language has been used.

General movement procedures are provided by G-Codes by using Marlin Firmware that has been developed for 3D Printers. The firmware allows the users to adjust velocity, acceleration, and jerk settings, gathering data via COM port to PC and if it’s necessary the firmware supports memory such as SD Cards. The sensor data and position data have been sent to PC to visualize magnetic flux map. Visualizing procedure is made at PC side by software that is developed in Python Programming Language and Matlab. In summary, purpose of "CMFM" are given below.

1.1 Magnetic Circuits

Magnetic circuits are made for reshape or reroute magnetic flux to achieve a goal such as collect ferromagnetic materials from bulk, amplify voltage. They could made from permanent magnets or electromagnets. In this study magnetic circuits those were made from permanent magnets have been studied. To build a magnetic circuit ferromagnetic materials (FM) were used with magnetic arrays. With FMs magnetic flux route could be reshaped and amplified to achieve Magnetic Force Index (MFI) to catch FMs those were desired geometry and from desired distance.

1.2 Magnetic Force Index (MFI)

A value that represents the magnetic force of attraction exerted by a magnet on a ferromagnetic object at a particular distance. As concerns attraction, it is the extent to which a magnetic field is inhomogeneous that determines its strength.

The MFI could be calculated with equation below.

$$MFI = B\frac{\Delta B}{\Delta x} \tag{1.1}$$

The more magnetic flux gradient, the more magnetic attraction force occurs. For attraction of ferrous material, the specific force index must be provided. Specific force index is function of shape, magnetic permeability of material and temperature.

Table 1.1 Specific force indexes of some materials

Object	**Specific Force Index**
Ball Ø 5 mm	3000
Ball Ø 25 mm	3000
Hex Nut M4(DIN934)	1900
Hex Nut M20(DIN934)	1900
Crown Closure	120
Nail Ø4.5x90 mm	90

1.3 Magnetic Separations and Magnetic Separators

The process of separating FMs from mixtures by using magnetic attraction is called magnetic separation, and the device that makes separation with this method is called magnetic separator (Oberteuffer, 1973). Magnetic circuits are commonly used for building this kind of separators.

Magnetic separators have wide range of uses in many industrial applications such as recycling, food, construction, etc. Magnetic separators branch two main branches by magnetic system made from permanent magnetic separators and electromagnetic separators. In this study, a way of quality control for permanent magnetic circuits those are used in permanent magnetic separators is studied.

Figure 1.1 An industrial magnetic separator (Imimg, n.d.)

1.4 Purpose of CMFM

Getting metal material or partials from waste or food bulk is an issue that getting importance day by day. And there are general using of magnetic separators. Both business areas are based on trust that between manufacturers of separators and the consumers. There isn't any mechanism to check their work. But there is measurement devices have developed newly.

Permanent magnet separator includes a magnetic circuit. The biggest design issue is designing of that circuit. If it doesn't have desired performance, the separator doesn't manage the task. The circuit plays vital role for make it right. The fail of the separator would cost to facility as punishment, unplanned downtime, loss of work time, money, etc. To guaranty of work and protect both sides, the performance of circuit must be measured and stored as 3D mapped report. That kind of stored data also used in analysis method as Discrete Element Method to simulating performance of separator and deciding side accessories performance.

CHAPTER TWO
MECHANICAL DESIGN

In this chapter, mechanical components of CMFM were mentioned in detail. After the parts are introduced in detail, the design stages will be mentioned. The mechanical design and analysis are made in Solidworks. Sheet metal parts are manufactured by laser cutting and press break method. Generally, on the shelf products are preferred such as sigma profiles, bearings, bearing supports, trigger pulleys etc. To design of sheet metal parts this standard machine dimensions of parts are used.

2.1 Mechanical Parts

2.1.1 Sigma Profiles

Sigma profiles are general use Machine manufacturing materials. They are made from generally 6000 series aluminum alloy, and anodized coating is applied. Thanks to the standard grooves on it, a structure can be made quickly by using special nuts and accessories. In this study 30x30 (Figure 2.1) and 20x20 (Figure 2.2) sigma profiles have been used.

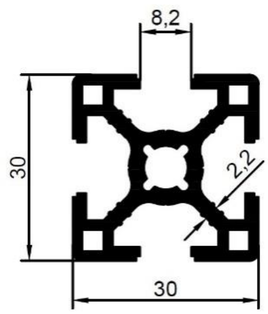

Figure 2.1 30x30 Sigma profile (Hksaluminyum, n.d.)

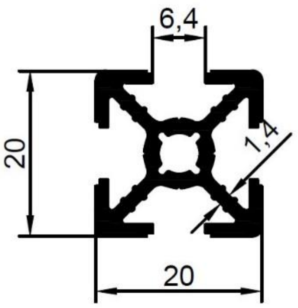

Figure 2.2 20x20 Sigma profile (Hksaluminyum, n.d.)

2.1.2 Hammer Nuts

Hammer nuts specialized nuts those are used for assembly of structures those are made from sigma profiles. These nuts are selected according to the size of my sigma profile to be used. Hammer nuts have striations unlike other nuts. Thanks to these striations when they were fastened, they deform inner surface of sigma profile, thus there occurred closed-form connection.

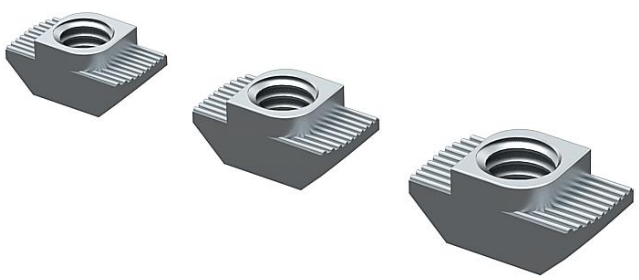

Figure 2.3 Hammer nuts (Doguskalip, n.d)

2.1.3 SCE Linear Ball Bearing Unit

One of the fundamental motions is linear motion. In a design to provide stability of linear motion, there must be a linear bearing. In this example to satisfy linear movement in one direction and also to figure out connection method of part linear ball bearing unit has been used. This bearing type provides rolling movement between contact surfaces rather than sliding.

Figure 2.4 SCE linear bearing unit (Tradebearings, n.d.)

Also, this member has variations for use in different circumstances. And a variant of this member has been used in this design, also. The selection criteria are linear position of the track and the rail relative to each other. In this selection both are parallel.

2.1.4 LMEF Linear Ball Bearing Unit

This member also works just like SCEs. Different from LMEFs, SCEs have flange that is used for fastening parts perpendicular to rail.

Figure 2.5 LMEF linear ball bearing unit (Radikalmuhendislik, n.d.)

2.1.5 Induction Hardened Linear Shaft (IHLS)

All linear bearing systems need rails. The rails have different cross section shapes such as rectangular, circular or special forms. The most cost-effective type is IHLS. They are basically rods made from heat treatable steel such as C45. And they heat treated by induction hardening method. With this method shafts' surfaces hardened but shafts' core is still soft. This kind of partial hardening ensures a good resilience.

Figure 2.6 Induction hardened linear shaft (Misumi-ec, n.d.)

2.1.6 SHF Linear Shaft Support

To generate precise linear motion, the rail must be fixed as possible as rigidly. To facilitate assembly and to ensure rigidity some on the shelf part can be found just like linear ball bearings.

SHFs are used for fixing linear shafts perpendicular to parts those support the shafts.

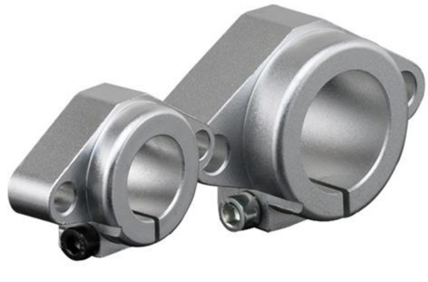

Figure 2.7 SHF linear shaft support (Cnballscrew, n.d.)

2.1.7 SK Linear Shaft Support

SKs are used for fixing linear shafts parallel to parts those support the shafts.

Figure 2.8 SK linear shaft support (Diyelectronics, n.d.)

2.1.8 Trapezoidal Screws and Nuts

Trapezoidal screw is a lead screw this is used as a linkage in a machine to translate turning motion to linear motion. And it has outlines as trapezoidal shape. Also, the screw needs special nut to translate rotational movement to translational movement. The special nut has thread that has outline female form of screw.

Generally, screws and nuts provides high gear ratio but also because property of connection they produce friction losses. But they are cost effective solutions rather than with ball versions.

Figure 2.9 Trapezoidal screw and variations of nuts (Amazon, n.d.)

2.1.9 UFL Bearing Unit

There are a lots of bearing units on the shelves to solve various rotational movement issues. Wise chose of one of them reduces the cost of machining and assembly. In this case because of minor amount of radial load and generally construction's loads are axial, thus two bolted pillow type bearing unit (UFL) is selected. This type is used when the shaft and the carrier are perpendicular to each other.

Figure 2.10 UFL bearing unit (Ebayimg, n.d.)

2.1.10 JM1 Flex Coupling

By definition of coupling is a device for connecting parts of machinery. Primary use of coupling is transferring power one and to another end. A good coupling must have several properties those are given bellow (Table 2.1).

JM1 couplings are also known as "servo coupling" designed such a spring. This design provides good flexibility to compensate misalignment of shafts.

Table 2.1 Properties of Good A Coupling

To damped vibration of rotating unit to connect driving and driven parts
To protect from overloading
To provide for misalignment of the shafts
To provide mechanical flexibility

Figure 2.11 JM1 flex coupling (Souqcdn, n.p.)

2.1.11 GT2 Trigger Pulley

Figure 2.12 GT2 trigger pulley (Palmar, n.d)

GT2 is a miniaturized type trigger pulley and belt model and this model, unlike others, has rounded edges on its teeth to reduce backlash and to increase precision.

GT2 is also very popular model for construction of 3D printers because of cost and size. And generally used with stepper motor that size is NEMA 17. With its setscrew pulley can be fixed easily.

2.1.12 GT2 Trigger Belt

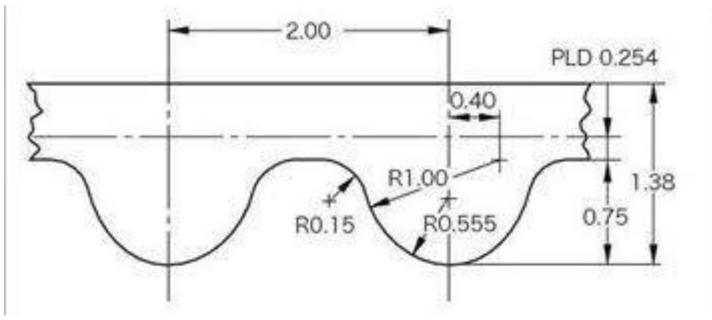

Figure 2.13 GT2 trigger belt (Adafruit, n.d.)

GT2 trigger belt also known as timing belt is designed specifically for linear motion. It has also rounded edges just like its pulley to reduce backlash and to increase precision.

2.1.13 Shoulder Bolt

Figure 2.14 Shoulder bolt (Bigcommerce, n.d.)

Shoulder bolt also known as shoulder screw designed as a pivot or linear guide considering the way of use. Generally, it is used in injection molding applications to guide molds linearly. Also, it is very effective as a pivot on linkages and gear mechanisms.

In this design, the shoulder bolt is used to pivot the GT2 pulleys excluding pulleys those are used with stepper motors.

2.1.14 Sheet Metal Parts

To connect and fix standard parts several sheet metal parts are designed. Some of parts includes multiple sheet metal bodies and some of the parts are bended thus to give those parts welding and bending techniques are used in addition to laser cut.

The parts are given below (Table 2.2).

Table 2.2 Sheet metal parts specifications

Part Visual	**Name**	**Method(s)**	**Part Code**
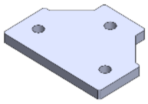	Profile Connection Plate	Laser Cut	P1
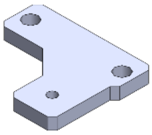	“L” Pulley Plate	Laser Cut	P2
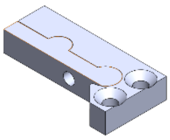	Belt Fixing Group	Laser Cut Countersink Operation Assembly	A1
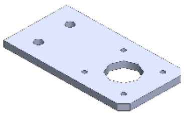	Stepper Support Plate	Laser Cut	P5
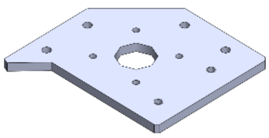	Corner Stepper Plate	Laser Cut	P6
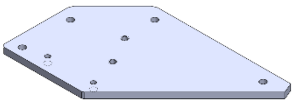	Corner Pulley Plate	Laser Cut	P7

Table 2.2 continues

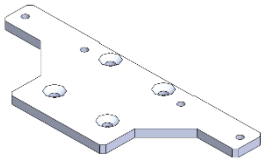	Y Axis Bearing Support Plate	Laser Cut Countersink Operation	P8
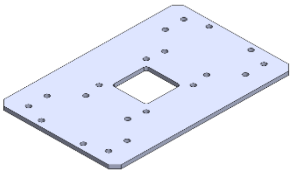	End Effector Plate	Laser Cut	P9
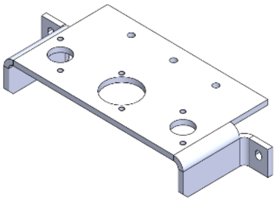	Bearing Support Plate	Laser Cut Press Break Bend	P10
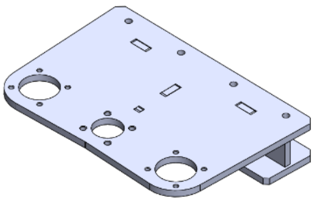	Actuator Part Weldment Group	Laser Cut Welding	W1

2.1.15 Hex Socket Bolt

To assemble the structure of CMFM hex socket bolt is used.

Figure 2.15 Hex socket bolt (Cloudfront, n.d.)

2.2 Mechanical Design

Generally, the design is inspired by CMM and 3D printers. The geometry of design is rectangular because of Cartesian movement of axis.

2.2.1 The Movement Approach through X and Y Axes

This part was thought to be 2 dimensional. Traditional design of 2D Cartesian one of axis carries mass of linear guides and actuating motor of another axis.

In this type of design, the motor of carrying axis must be powerful than the other axis because of inertia. And also, linear guides of carrying axis must be bigger than the other. To avoid that situation and for a lighter design Core XY approach is decided (Figure 2.16).

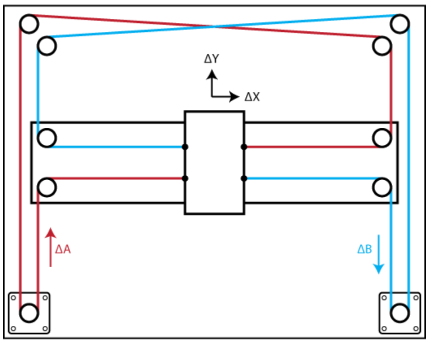

Figure 2.16 Core XY schema

$$\Delta X = \frac{\Delta A + \Delta B}{2} \tag{2.1}$$

$$\Delta Y = \frac{\Delta A - \Delta B}{2} \tag{2.2}$$

$$\Delta A = \Delta X + \Delta Y \tag{2.3}$$

$$\Delta B = \Delta X - \Delta Y \tag{2.4}$$

The equations about the movement is given above. It was assumed that the differential motions in the direction of X and Y axes were ΔX and ΔY. And these motions were performed by stepper motor A and ΔA and ΔB were differential linear motions those were provided by stepper motors A and B. The relationships between ΔX, ΔA and ΔB is given at Equation 2.1 and between ΔY, ΔA and ΔB is given at Equation 2.2. Equations 2.3 and 2.4 are obtained from the common solution of equations 2.1 and 2.2. These expressions are the expressions of how much motion the motors must produce to provide ΔX and ΔY. It is seen that the Cartesian movement obtained based on the equations obtained in the result is a movement rotated 45 degrees with respect to the movement in the modified axes A and B.

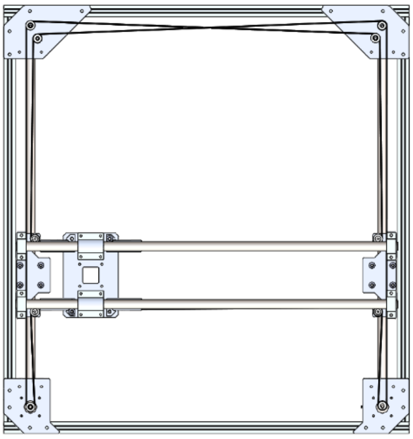

Figure 2.17 Top view of X-Y axes

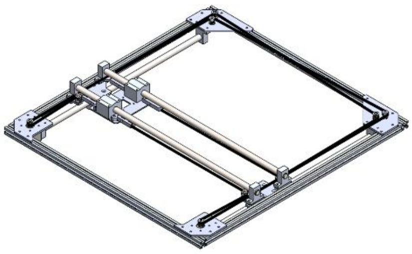

Figure 2.18 Isometric view of X-Y axes

2.2.2 The Movement Approach through Z Axis

In this part was thought to be 1 dimensional. To provide linear movement pair of lead screw has been used.

In this type of design rotational motion of motors are transformed into linear motion. But it is very important to mind bearing and lead screw - nut clearance (Figure 2.8). If those were arranged wrongly, the movement would be jammed somewhere in its stroke.

To avoid the jamming issue, the clearance of linear bearing is selected less than clearance of lead screw-nut. Thus the radial load that occurs at the moment of motion is borne by linear bearing (Figure 2.5).

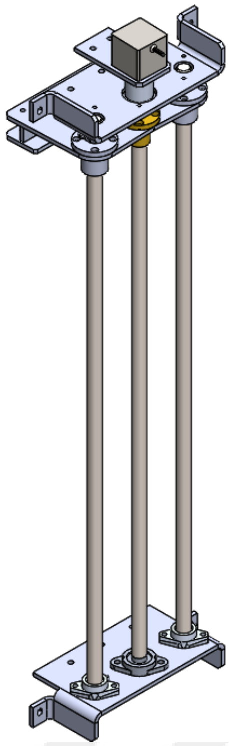

Figure 2.19 Isometric view of one of z axis actuators

2.2.3 Full Assembly of CMFM

The external dimensions of the CMFM after assembly are given below (Table 2.3).

Table 2.3 External dimensions of CMFM in mm.

Width	**Depth**	**Height**
930	740	835

The dimensions of the workspace are given below (Table 2.4).

Table 2.4 Dimensions of the workspace in mm

Width	**Depth**	**Height**
600	303	640

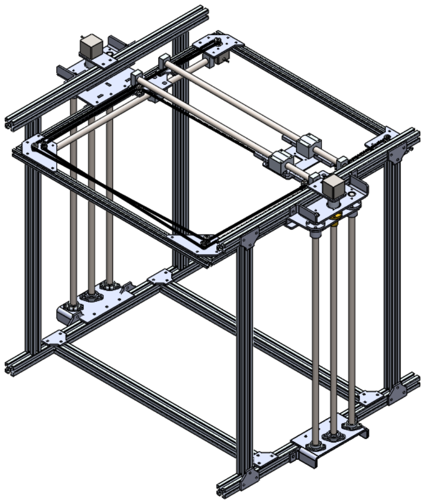

Figure 2.20 Isometric view of CMFM

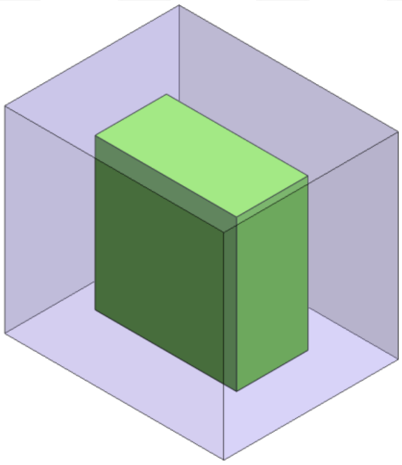

Figure 2.21 Comparison of CMFM's volume and workspace

The comparison of CMFM's volume and workspace is shown above. The volume of CMFM is shown as greyish purple and workspace is shown in green.

The ratio between volumes is given below (Equation 2.5).

$$i_{vol} = \frac{V_{workspace}}{V_{CMFM}} = \frac{600 \ x \ 303 \ x \ 640}{930 \ x \ 740 \ x \ 835} \approx 20\% \tag{2.5}$$

CHAPTER THREE

ELECTRICAL COMPONENTS AND DESIGN

In this chapter, electrical elements and their properties are mentioned. The RepRap 1.4 kit, which is used generally for 3D printers, has been used with minor hardware and software modifications.

3.1 Electrical Components

3.1.1 Arduino Mega 2560 Rev3

3.1.1.1 Arduino

Arduino is a company that produces open source hardware and software. The boards those are produces by Arduino includes several types of structured microcontroller such as Atmel AVR, ARM Cortex, and Intel Quark. Arduino is technically fed from communities.

3.1.1.2 Arduino Integrated Development Environment (IDE)

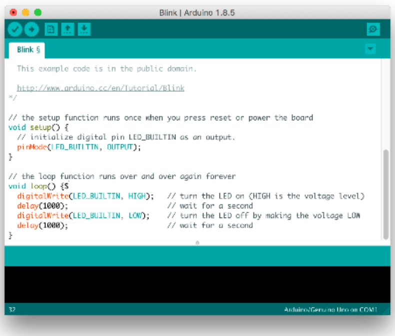

Figure 3.1 Arduino IDE user interface (Wikipedia, n.d.)

"The Arduino Family" has own integrated development environment (IDE) that is suitable for all products that is provided by Arduino. The IDE is also very resourceful, and it has easy to reach documents, examples and tutorials. Those elements make it selectable.

3.1.1.3 The Board

“Arduino Mega 2560”is a microcontroller board that includes Atmega 2560 microcontroller. “The RepRap 1.4” kit is compatible with this board's inputs and outputs. This card has USB port on it to communicate with a computer by using serial port protocol. It can be easily programmed with low performance computer.

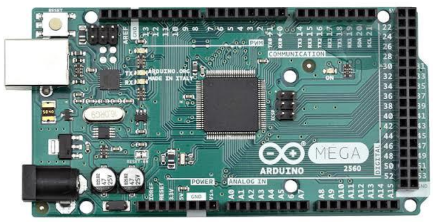

Figure 3.2 Arduino Mega 2560 development board (Arduino, n.d.)

3.1.2 RepRap Project

The RepRap is an initiative to manufacture low-cost 3D printers that is started by University of Bath in England in 2005. RepRap is short for **rep**licating **rap**id prototype.

The project includes several open source hardware and software to satisfy technical needs a fundamental 3D printer.

Software side of the RepRap project include drivers for electrical components such as stepper drivers, LCD screens etc. Those are developed in C and C++ programming languages. Most popular firmware is Marlin.

3.1.2.1 RepRap 1.4 Shield

The RepRap Shield is very popular in 3D printer community. This card is capable of 5 stepper motors and multiple analog sensors at the same time. Card's driver software, documentation, examples and tutorials also found easily. There is a lots of project those have potential to inspire for another projects on internet.

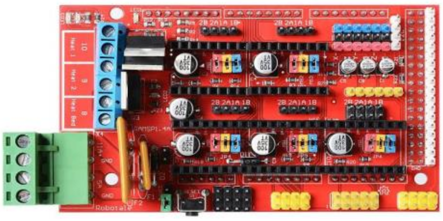

Figure 3.3 RepRap 1.4 shield (Miniinthebox, n.d.)

3.1.2.2 RepRap 12864 LCD Smart Display

This Smart Controller contains a SD-Card reader, a rotary encoder and a 20 Character x 4 Line LCD display. You can easily connect it to your RepRap 1.4 Shield.

This screen provides a user interface. Maximum speed, acceleration, jerk parameters can be accessed, SD card can be inserted, and instant position information can be seen through this screen.

Figure 3.4 RepRap 12864 LCD smart display (Miniinthebox, n.d.)

3.1.2.3 Marlin Firmware

Marlin is open source firmware that is developed for Arduino based 3D printers generally RepRap. With this firmware coordinate type, length of axis, limits can be configured.

Figure 3.5 The logo of marlin firmware (Marlinfw, n.d.)

3.1.3 A4988 Stepper Motor Driver

The A4988 is a complete micro stepping motor driver with built-in translator for easy operation. It is designed to operate bipolar stepper motors in full-, half-, quarter-, eighth-, and sixteenth-step modes, with an output drive capacity of up to 35 V and ±2 A. The A4988 includes a fixed off-time current regulator which has the ability to operate in Slow or Mixed decay modes.

In this case the driver has own shield that is compatible with RepRap 1.4 kit (Figure 3.6). With this specialty it is very popular in 3D printer’s community. Generally, stepper motors in this kind of project are driven with this integrated circuit. It has built in current limiter to protect itself. When it is connected to stepper motor current limiter must be tuned for stepper motor specifically.

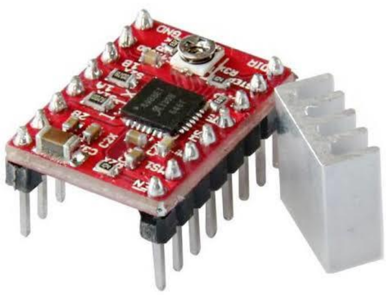

Figure 3.6 A4988 stepper motor driver (Google, n.d.)

3.1.4 NEMA 17 Stepper Motor

The most common stepper motor on the 3D printer community. It is cheap, small, and easy to find motor for any kind of projects. I have 200 steps per revolution. It means the motor has 1.8-degree step angle. Thanks to stepper driver A4988 it can be driven with micro steps such as sixteenth-step mode. Thus, step angle is reduced to 0.1125 degree. It increased precision.

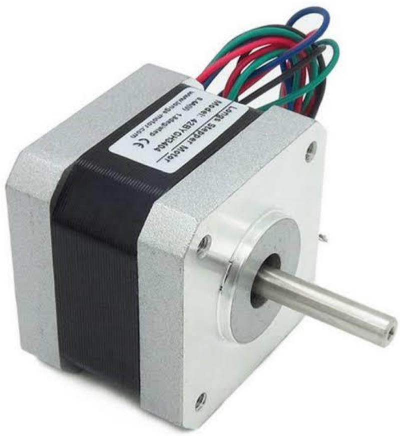

Figure 3.7 NEMA 17 stepper motor (Google, n.d.)

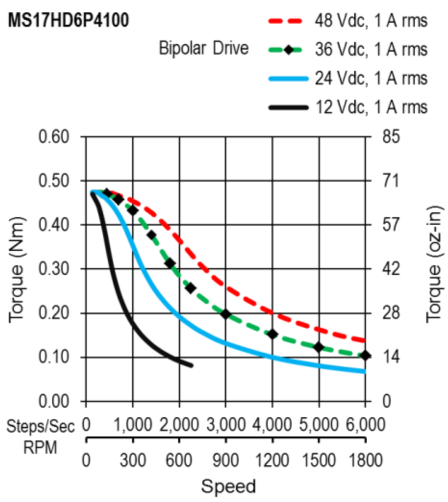

Figure 3.8 NEMA 17 rpm to torque diagram (Google, n.d.)

According to diagram above (Figure 3.8) in this application this motor generates approximately 0.45 to 0.1 Nm torque.

3.1.5 Power Supply 12V 200W

To operate all of electrical component DC voltage is required. Power supply provide that voltage regulated and safe. To operate the system 12 V and 200 W power supply is selected according to recommendation from RepRap project's documentation.

Figure 3.9 Power supply 12V 200W (Makerlab-electronics, n.d.)

3.1.6 Sensing the Magnetic Flux

One of common method to measure magnetic flux is using Hall Effect sensor. A Hall Effect sensor is a device that is used to measure the magnitude of a magnetic field. By phenomena is called Hall Effect. The Hall Effect is the production of a voltage difference a cross an electrical conductor, transverse to an electric current in the conductor and to an applied magnetic field perpendicular to the current (Diodes, 2019).

But using this phenomena n a magnetic field sensing electronically circuit it must be linear. It means magnitude of the magnetic field that is applied on sensor and magnitude of the output voltage of sensor must be proportional.

3.1.6.1 Hall Effect Sensor AH49H

The AH49H is a small, versatile linear Hall-effect device that is operated by the magnetic field from a permanent magnet or an electromagnet. The output voltage is set by the supply voltage and varies in proportion to the strength of the magnetic field.

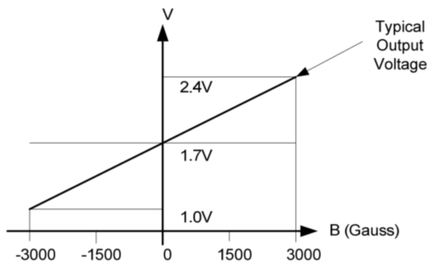

Figure 3.10 Transferring characteristic of ah49h at 3.3v source voltage (Diodes, n.d.)

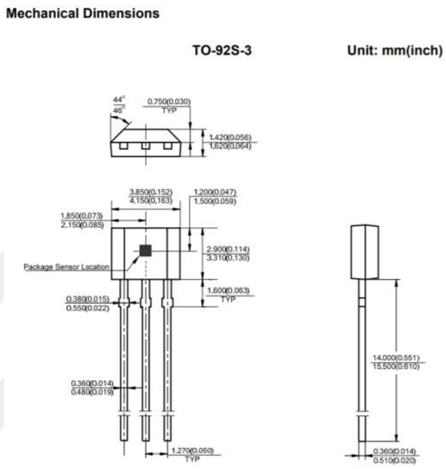

Figure 3.11 Mechanical dimensions of AH49H (Diodes, n.d.)

3.1.6.2 Design of the Interface Op Amp Circuit

To begin the design of the op amp circuit. The op amp must be chosen. The main criteria is linearity of the op amp. The input voltage range 1 to 2.4 V (Figure 3.12), thus in this range op amp must show linear behavior. According to Texas Instruments documents and ease to find TL072 has been chosen for this task.

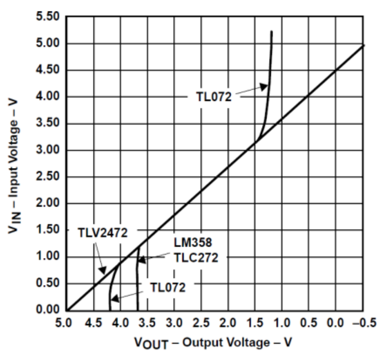

Figure 3.12 Linearity behaviors of several op amps (Ti, 2001)

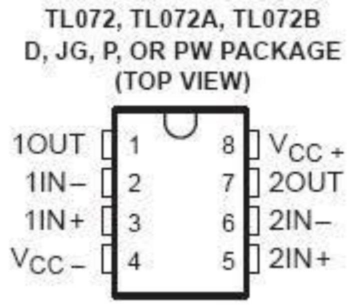

Figure 3.13 TL072 op amp schema (Ti, n.d.)

And the output voltage range has been chosen as 1 to 4.5 V because the analog to digital converter of Arduino Mega 2650 has range of 0 to 5 V. The circuit designs are like that limit values are avoided. And it is also used to set resistor values to standard values.

Taking an orderly path to developing a circuit that works the first time starts here; follow these steps until the equation of the op amp is determined. Use the specifications given for the circuit coupled with simultaneous equations to determine what form the op amp equation must have. Go to the section that illustrates that equation form (called a case), solve the equation to determine the resistor values, and you have a working solution. A linear op-amp transfer function is limited to the equation of a straight line (OpAmp Texas Ins. Single OpAmp Technique, 2019).

$$y = \pm mx \pm b \tag{3.1}$$

Thus, according to Equation 3.1 there is four possibilities because of signs.

$$V_{out} = +mV_{in} + b \tag{3.2}$$

$$V_{out} = +mV_{in} - b \tag{3.3}$$

$$V_{out} = -mV_{in} + b \tag{3.4}$$

$$V_{out} = -mV_{in} - b \tag{3.5}$$

$$V_{out_1} = +mV_{in_1} + b \tag{3.6}$$

In order to continue, it is determined which group of signs matches this situation. According to input and output voltages and assuming all signs are positive linear solution is given below.

$$V_{out_2} = +mV_{in_2} + b \tag{3.7}$$

$$\begin{bmatrix} V_{in_1} & 1 \\ V_{in_2} & 1 \end{bmatrix} \begin{bmatrix} m \\ b \end{bmatrix} = \begin{bmatrix} V_{out_1} \\ V_{out_1} \end{bmatrix} \tag{3.8}$$

$$\begin{bmatrix} m \\ b \end{bmatrix} = \begin{bmatrix} V_{in_1} & 1 \\ V_{in_2} & 1 \end{bmatrix}^{-1} \begin{bmatrix} V_{out_1} \\ V_{out_1} \end{bmatrix} \tag{3.9}$$

Table 3.1 Initial values of circuit design in volts

State	**V_{in}**	**V_{out}**
1	1	1
2	2.4	4.5

Plugging into Equation 3.9 values in Table (3.1)

$$\begin{bmatrix} m \\ b \end{bmatrix} = \begin{bmatrix} 1 & 1 \\ 2.4 & 1 \end{bmatrix}^{-1} \begin{bmatrix} 1 \\ 4.5 \end{bmatrix} \tag{3.10}$$

$$\begin{bmatrix} m \\ b \end{bmatrix} = \frac{1}{1x1 - 1x2.4} \begin{bmatrix} 1 & -1 \\ -2.4 & 1 \end{bmatrix} \begin{bmatrix} 1 \\ 4.5 \end{bmatrix} \tag{3.11}$$

$$\begin{bmatrix} m \\ b \end{bmatrix} = \begin{bmatrix} 2.5 \\ -1.5 \end{bmatrix} \tag{3.12}$$

Thus, this situation refers to Equation 3.3 because of signs. Generalized circuit of the equation is given below.

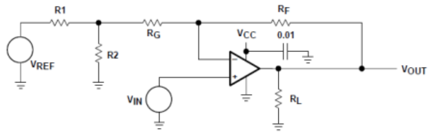

Figure 3.14 Schematic for equation 3.3

The circuit equation is obtained by taking the Thevenin equivalent circuit looking into the junction of R1 and R2. After the R1, R2 circuit is replaced with the Thevenin equivalent circuit, the gain is calculated with the ideal gain equation 3.13.

$$V_{out} = V_{in}\left(\frac{R_F + R_G + R_1||R_2}{R_G + R_1||R_2}\right) - V_{ref}\left(\frac{R_2}{R_1 + R_2}\right)\left(\frac{R_F}{R_G + R_1||R_2}\right) \quad (3.13)$$

Comparing terms in Equation 3.13 and Equation 3.3 enables extraction of m and b.

$$m = \frac{R_F + R_G + R_1||R_2}{R_G + R_1||R_2} \quad (3.14)$$

$$|b| = V_{ref}\left(\frac{R_2}{R_1 + R_2}\right)\left(\frac{R_F}{R_G + R_1||R_2}\right) \quad (3.15)$$

“m” and “b” has been found in Equation 3.12. Assuming that $R_1||R_2 \ll R_G$ simplifies the calculations the resistor values (TI, 2001).

Let $R_L = 10k\Omega$, $V_{ref} = V_{cc} = 5V$

“m” and “b” has been found in Equation 3.12. Assuming that $R_1||R_2 \ll R_G$ simplifies the calculations the resistor values.

$$m = 2.5 = \frac{R_F}{R_F + R_G} \quad (3.16)$$

$$R_F = 1.5R_G \quad (3.17)$$

Let $R_G = 20k\Omega$, and then $R_G = 30k\Omega$.

$$b = 5\left(\frac{R_F}{R_G}\right)\left(\frac{R_2}{R_1 + R_2}\right) = 5(1.5)\left(\frac{R_2}{R_1 + R_2}\right) = 1.5 \quad (3.18)$$

$$R_1 = 4R_2 \tag{3.19}$$

Let $R_2 = 1k\Omega$, and then $R_2 = 4k\Omega$. Thus $R_1||R_2 = 0.8\ k\Omega . R_G \gg R_1||R_2$ is justified.

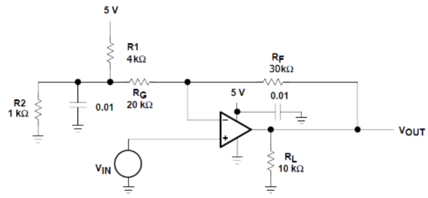

Figure 3.15 Interface Circuit Schema

The real-world output of circuit will be examine in “Results” section.

CHAPTER FOUR
ANALYSIS

Before starting of analysis, positions of end effector are decided and named systematically.

4.1 Naming of Positions

The First Letter of code refers to position of end effector (EE) along the “z” axis. For this letter there are three alternatives “d” for bottom” for middle, and “u” for top position. The Second Letter refers to position of EE along the “x” axis. For this letter there are three alternatives “s” for maximum value of “x” it refers to “south”, “m” for middle, and “n” for minimum value of “x” it refers to “north”. The Third Letter of code refers to position of EE along to “y” axis. For this letter there are two alternatives “l” for maximum and minimum value of “y” and “m” for “middle”. There is only one letter for maximum and minimum of “y”, because construction has a symmetry plane parallel to “XZ” plane. So, there will be same vibrations characteristic (Figure 4.1).

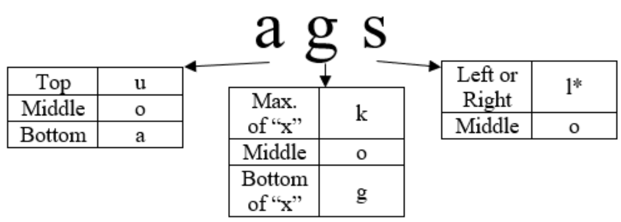

Figure 4.1 Naming methodology schema of positions

4.2 Simplifications for Analysis

To reduce computational work some simplifications has been made in CAD model. The design was symmetrical, but the design was avoided because the analysis was repeated at various positions of the "End effector".

The simplifications can be examined in two parts; CAD model changes and part reduction.

4.2.1 CAD Model Changes

To reduce mesh, count several CAD changes has been applied. Generally removing circular shapes is recommended such as drill holes but in this study most of drill holes has been not removed because of mate relationships.

Most of changes have been done on chamfers and radius. The changes has been given in Table 4.1 below.

Table 4.1 List of CAD changes those have been done

Part Visual	**Changed Part Visual**	**Changes**	**Part Code**
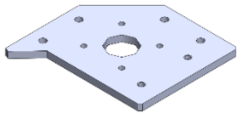	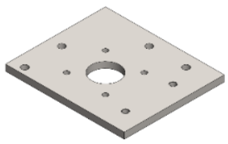	Chamfers are removed	P6
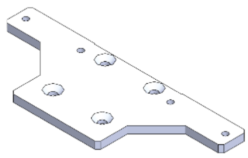	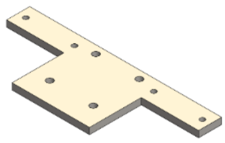	Chamfers are removed	P8
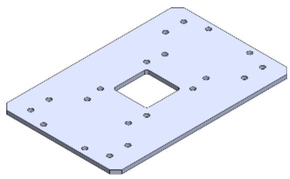	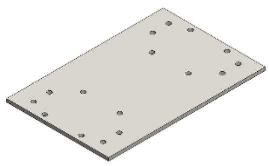	Inner void is removed	P9
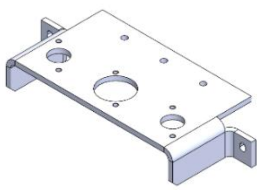	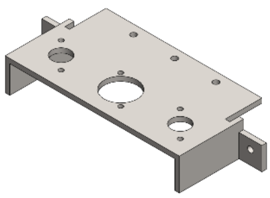	Bending radius are removed	P10

Table 4.1 continues

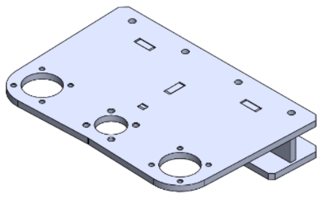	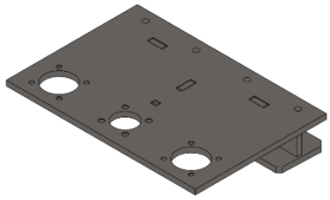	Radius are removed	W1
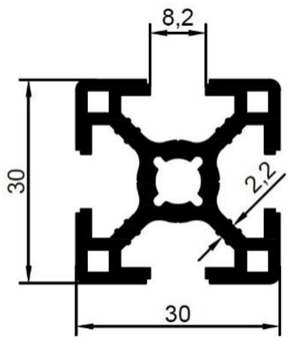	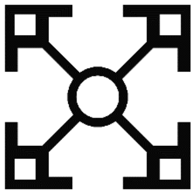	Several geometric reductions have been done	30x30 Sigma Profile
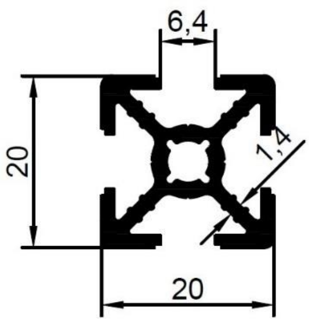	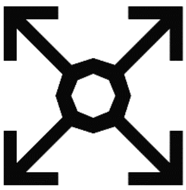	Several geometric reductions have been done	20x20 Sigma Profile

4.2.2 Part Reduction

Parts with mixed geometry without structural effect were reduced to point load to reduce the number of mesh.

Since it is a methodological study, both geometric simplification and point load acceptance have been made specifically for "P9" part.

The part reductions has been given in Table 4.2 below.

Table 4.2 List of part reductions

Part Visual	**Changed Part Visual**	**Specification**
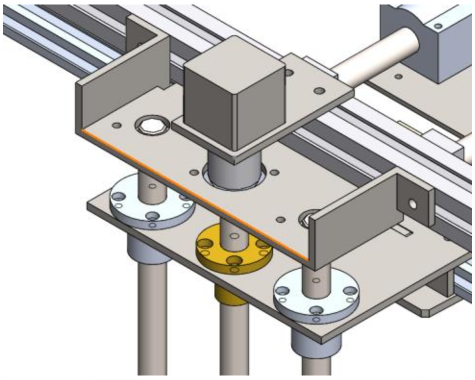	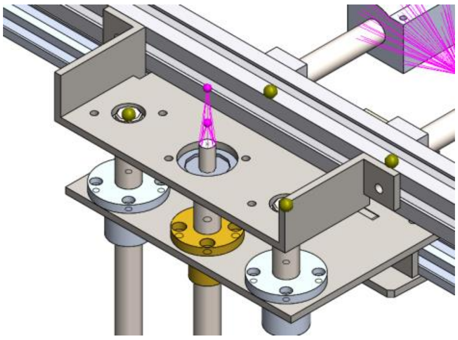	Stepper motor, Coupling and P5 are reduced to point loads.
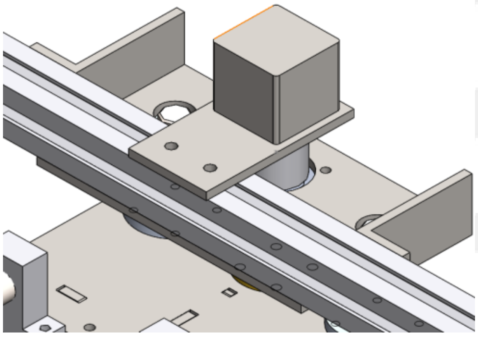	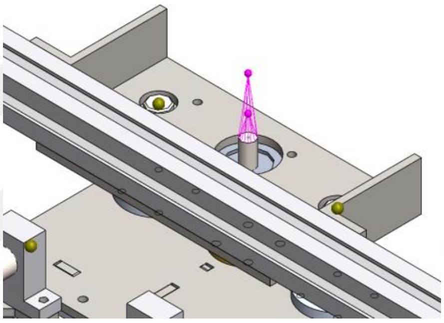	Stepper motor, Coupling and P5 are reduced to point loads.
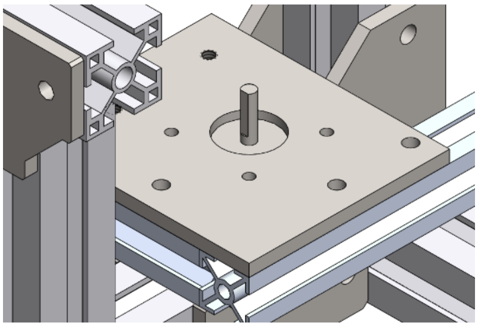	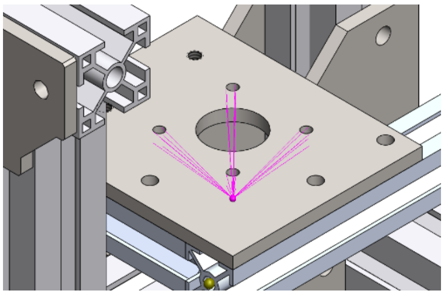	Stepper motor is reduced to a point load.

Table 4.2 continues

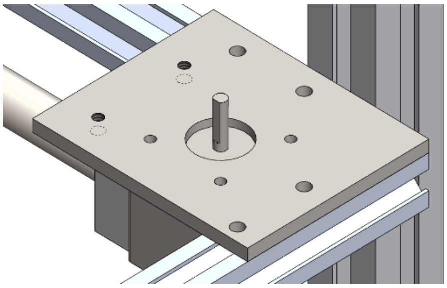	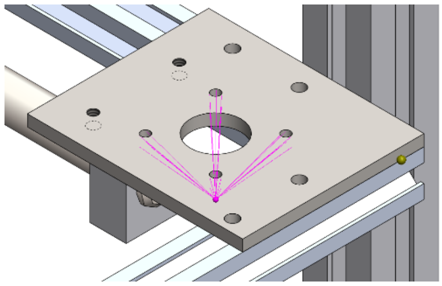	Stepper motor is reduced to a point load.
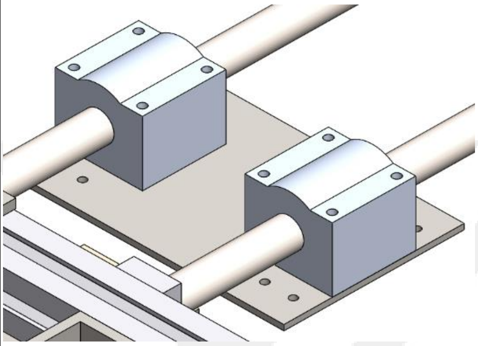	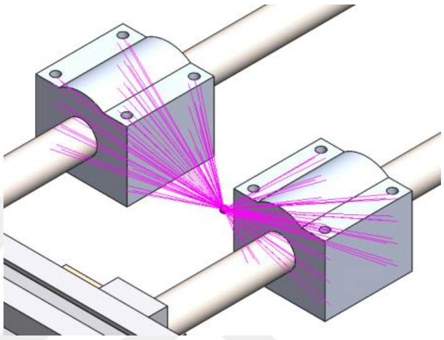	P9 is reduced to a point load.

4.3 Boundary Conditions

In Finite Element Analysis (FEA) at least one boundary condition must be declared. The condition has been given below in Figure 4.2. The bottom surface of chassis has been declared as fixed.

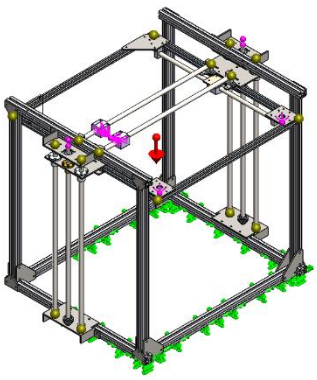

Figure 4.2 The boundary condition has been visualized by green arrows and gravity has been visualized by red arrow.

4.4 External Load

The gravity has been declared as an external load to liven up real-world conditions. The condition has been given above in Figure 4.2.

4.5 Mesh Controls

Several specific mesh controls have been applied due to failures those have been occurred while meshing process. One of cause of meshing failure was large mesh size. Because of various shapes there couldn't be defined fixed mesh size. The other cause is mate relations. Because of several of different relations some of sheet parts couldn't be declared as shell and some of beam parts couldn't be defined as beam.

List of mesh controls have been given below Table 4.3.

Table 4.3 Mesh Details

	Mesh Width	**Height/Width**
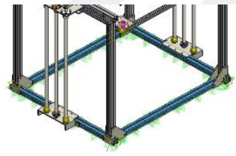	5	1.5
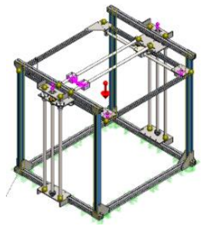	5	1.5
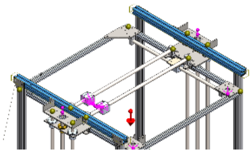	10	3

Table 4.3 continues

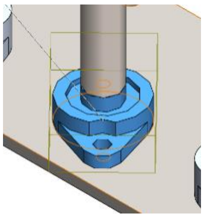	5	1.5
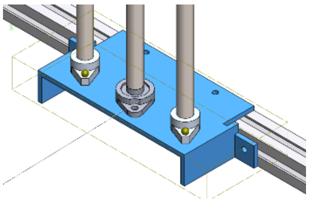	3	1.5
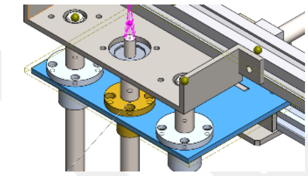	3	3
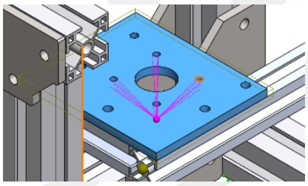	2	1.5
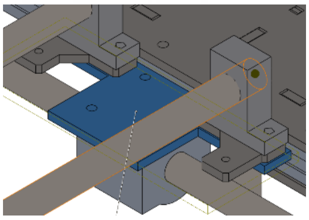	1	1.5

At Table 4.3 some of variables are same. Because when all those parts were united same mesh control familiar mesh failures were occurred again.

4.6 Static Structural Analysis

Since "CMFM" operates against its own weight, no dangerous stress and strain is envisaged. However, it is important to conduct analyzes to verify. In this design, displacement under gravity forces is more important than in other cases since position control is performed. The analysis results according to the naming methodology in subsection 4.1 are given in separate tables.

4.6.1 Stress Analysis Results

Stress is the ratio of applied force to a cross section area. There is three main type of stress; tensile stress, compressive stress and shear stress. Thanks to FEA analysis there could be seen stress resultant on any finite elements. The stress resultant of particular to cross-section have given below in Table 4.4.

Table 4.4 The list of stress analysis visuals

Position Name	**Stress Analysis Visual**
ako	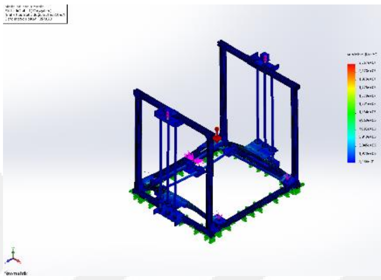
aks	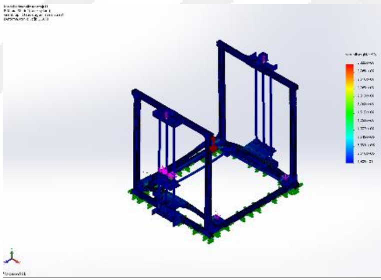
aoo	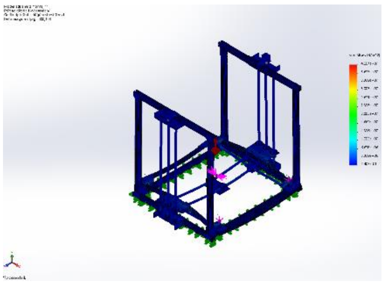

Table 4.4 continues

aos	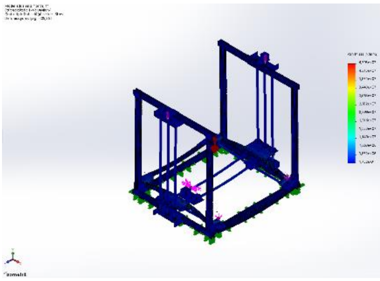
oko	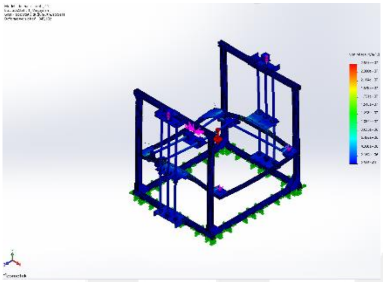
oks	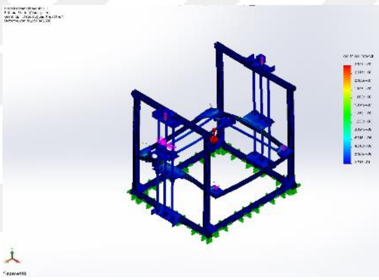
ooo	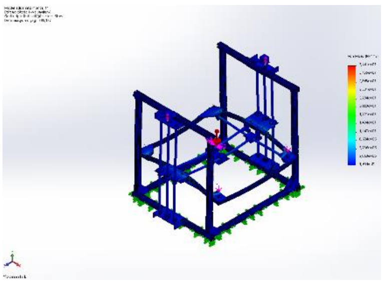
oos	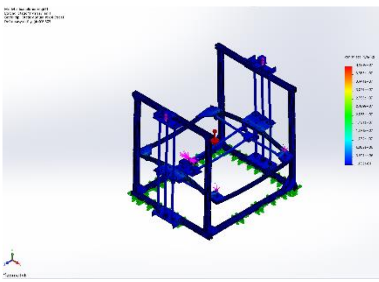

Table 4.4 continues

uko	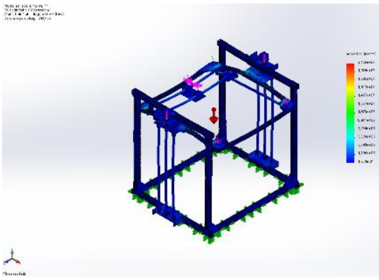
uks	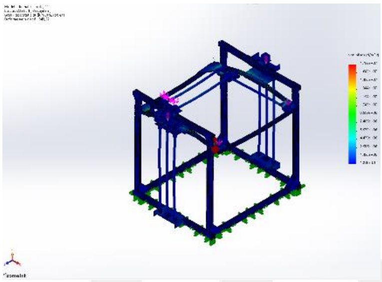
uoo	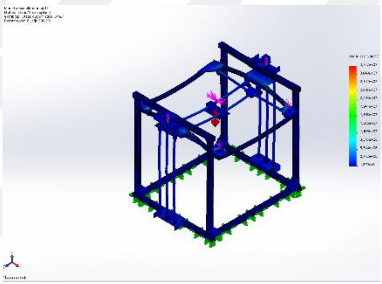
uos	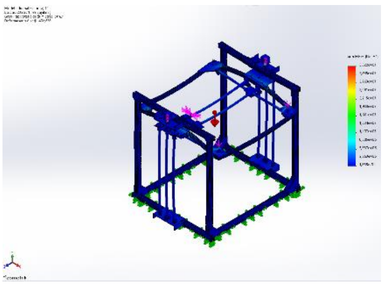

4.6.2 Strain Analysis Results

Objects those are under stress deforms and the ratio of diffraction of dimension to the initial dimension is called strain. The strain results of particular to cross-section have given below in Table 4.5.

Table 4.5 The list of strain analysis visuals

Position Name	**Strain Analysis Visual**
ako	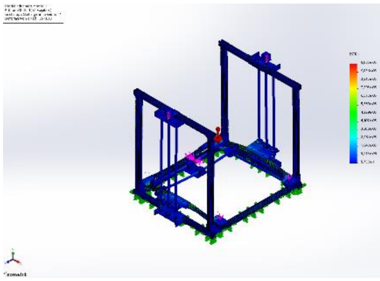
aks	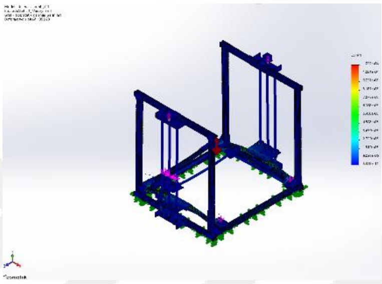
aoo	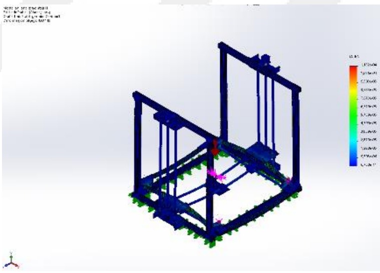
aos	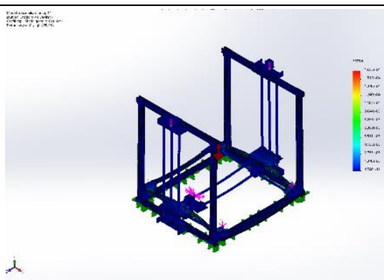

Table 4.5 continues

oko	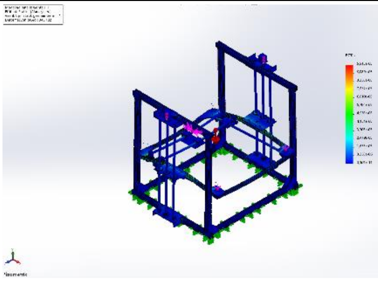
oks	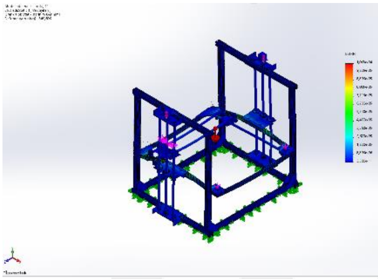
ooo	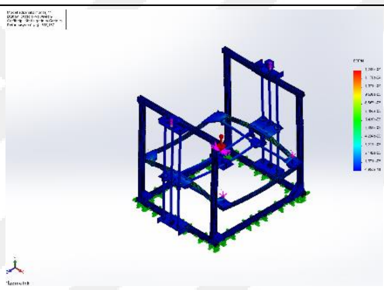
oos	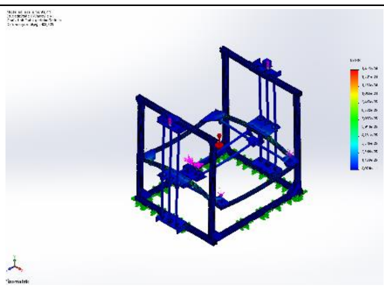
uko	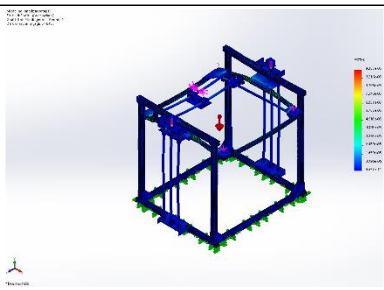

Table 4.5 continues

uks	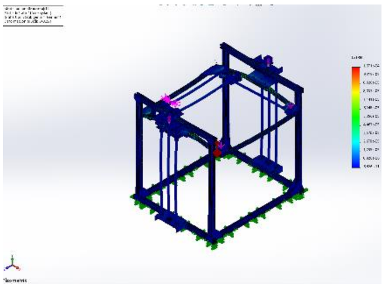
uoo	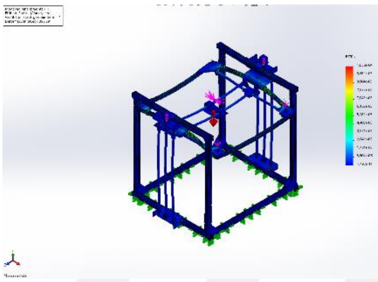
uos	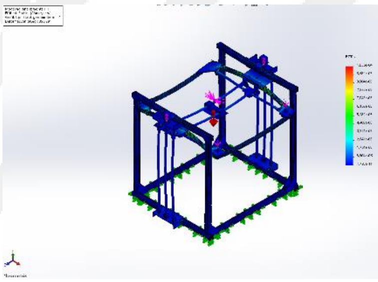

4.6.3 Displacement Analysis Results

Under force objects deform. The displacement results of particular to cross-section have given below in Table 4.6.

Table 4.6 The list of displacement analysis visuals

<u>Position Name</u>	**<u>Displacement Analysis Visual</u>**
ako	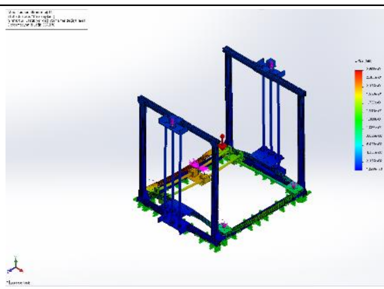

Table 4.6 continues

aks	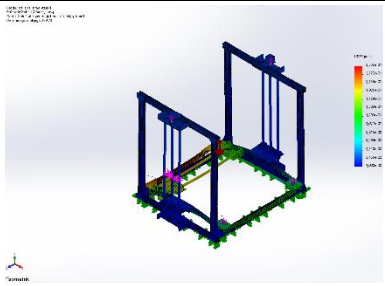
aoo	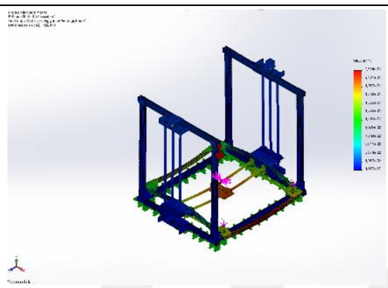
aos	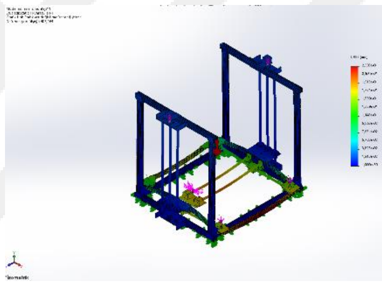
oko	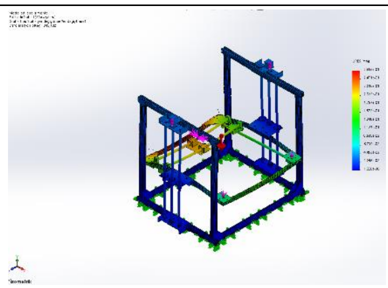
oks	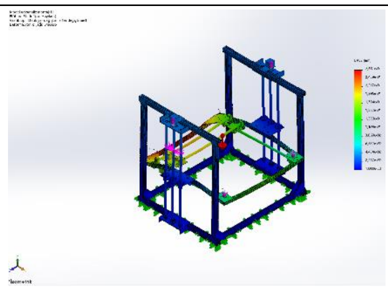

Table 4.6 continues

ooo	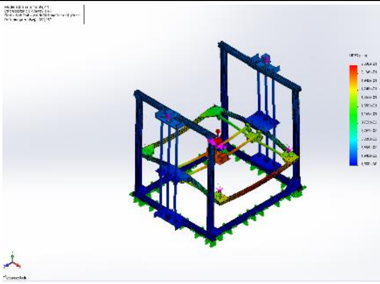
oos	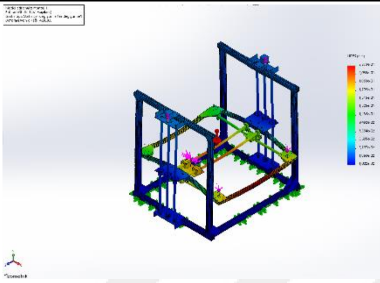
uko	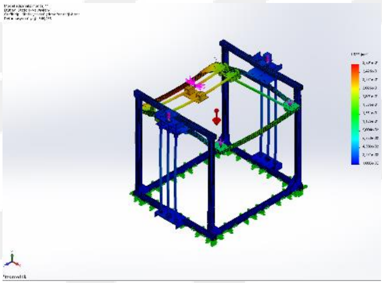
uks	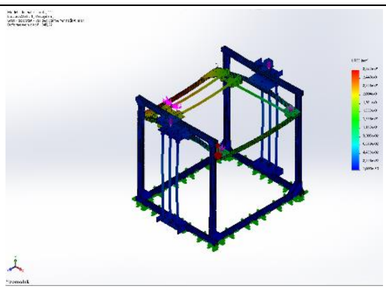
uoo	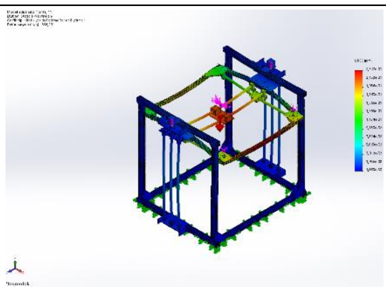

Table 4.6 continues

uos	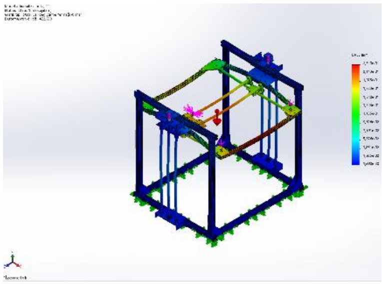

4.6.4 Summary of Static Structural Analysis

The maximum and the minimum value of results have been given below in Table 4.7.

Table 4.7 The list of maximum and minimum results

	Max Pos.	**Max Value**	**Min Pos.**	**Min Value**
Stress	aos	46 MPa	uks	18 MPa
Strain	uko	$1.1x10^{-4}$	ako	$9.4x10^{-5}$
Displacement	oko	$2.7x10^{-1}$ mm	oos	$2.3x10^{-1}$ mm

4.7 Modal Frequency Analysis and Impact Hammer Test

Resonance frequency of chassis is very important fact for a measuring devices such as CMFM. Because at the moment of measuring vibrations those were heavily effect the position of end effector wouldn't wanted. To see the vibration patterns of several positions those mentioned in subtitle 4.1 Modal Frequency Analysis was done for first five mode shapes.

Figure 4.3 The mode shapes of the system (Left to right are F1 to F5)

4.7.1 Results of Modal Frequency Analysis

Table 4.8 List of modal frequency analysis results for first five mode shapes

Pos. Name	**F1**	**F2**	**F3**	**F4**	**F5**
ako	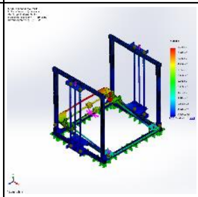	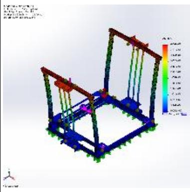	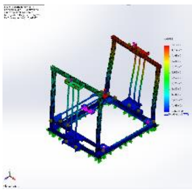	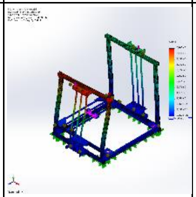	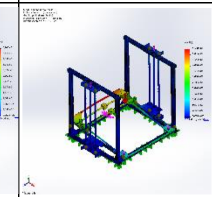
aks	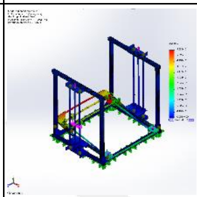	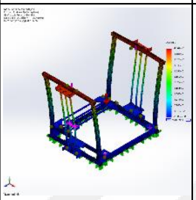	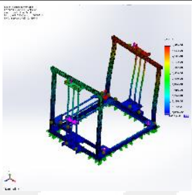	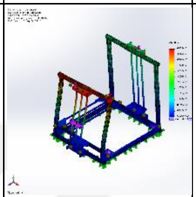	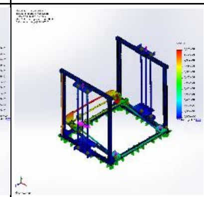
aoo	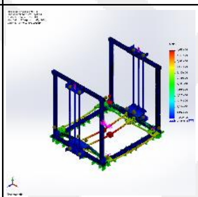	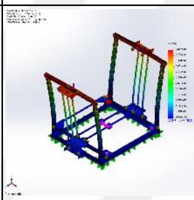	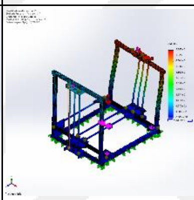	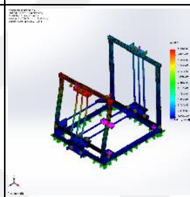	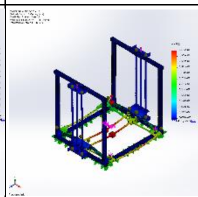
aos	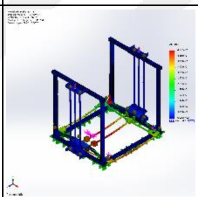	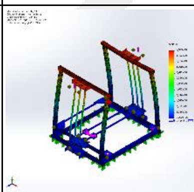	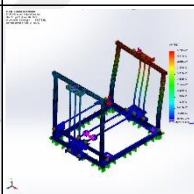	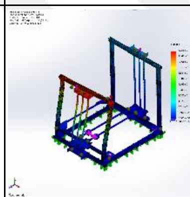	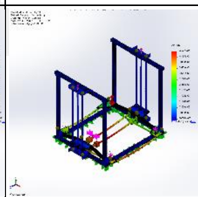
oko	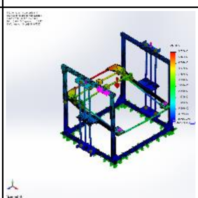	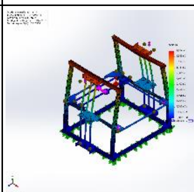	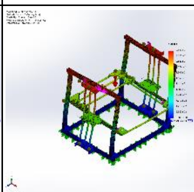	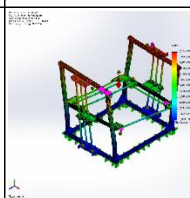	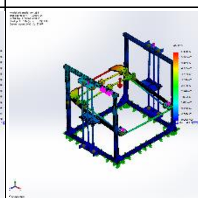
oks	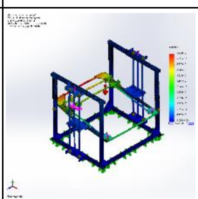	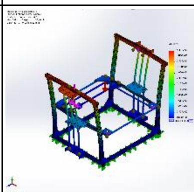	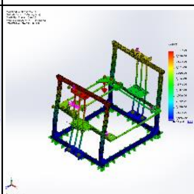	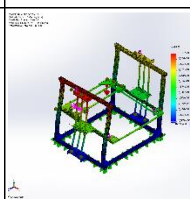	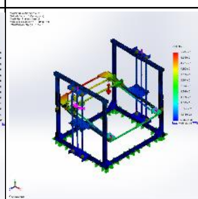
ooo	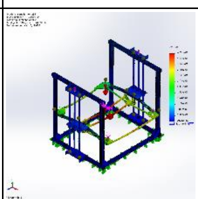	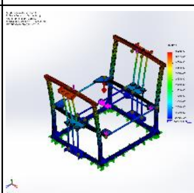	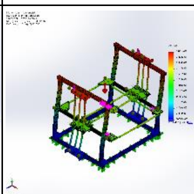	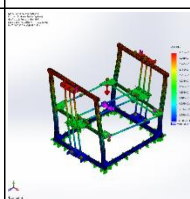	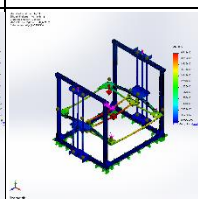

Table 4.8 continues

oos	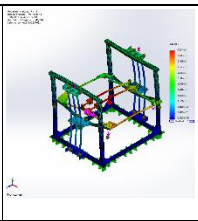	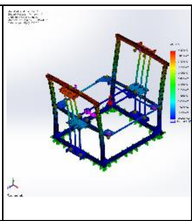	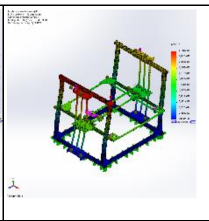	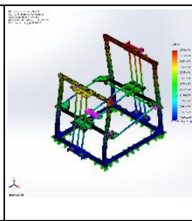	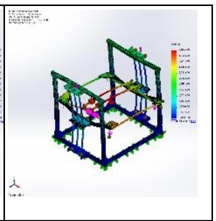
uko	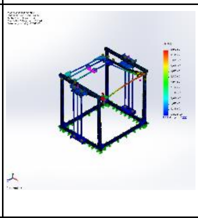	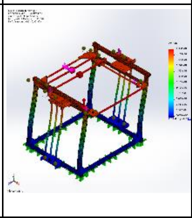	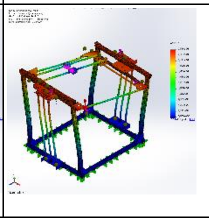	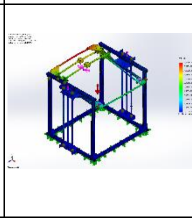	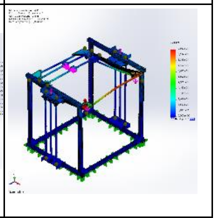
uks	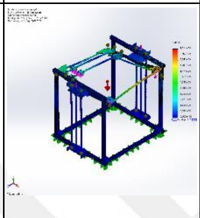	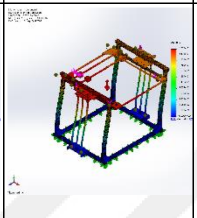	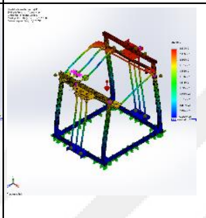	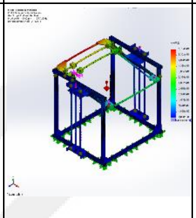	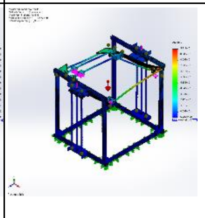
uoo	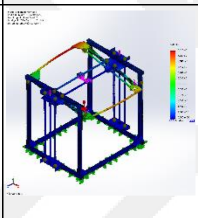	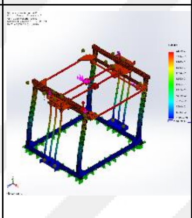	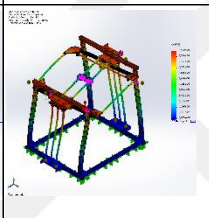	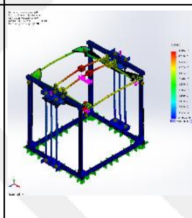	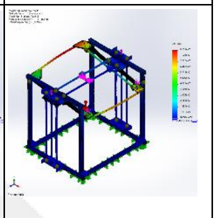
uos	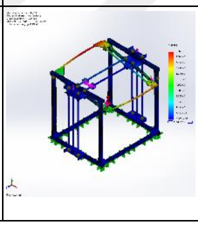	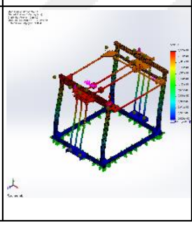	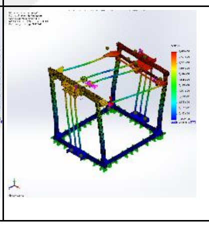	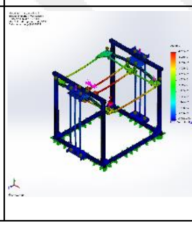	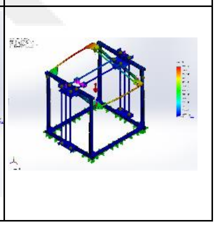

4.7.2 Summary of Modal Frequency Analysis

Table 4.9 Mode shape frequencies for specific positions.

Pos. Name	**F1**	**F2**	**F3**	**F4**	**F5**
ako	39.58	22.49	34.76	34.81	39.58
aks	40.1	22.49	34.76	34.8	40.1
aoo	45.12	22.48	34.78	34.81	45.12
aos	45.73	22.48	34.78	34.81	45.73
oko	39.12	30.68	34.81	38.91	39.12
oks	39.64	30.68	34.85	38.02	39.64
ooo	44.7	30.53	34.88	39.21	44.7
oos	45.22	30.52	35.93	38.18	45.22

Table 4.9 continues

uko	53.54	21.25	30.23	38.93	53.54
uks	52.72	21.26	27.96	39.43	52.72
uoo	51.16	21.24	30.77	44.41	51.16
uos	51.14	21.25	28.24	45.01	51.14

On that “Table 1” Bellow of 30 Hz are displayed in light red background color. This case some of positions there are below 30 Hz mode shape frequencies according to Table 4.9. Most of bellow 30 Hz situations are seen at second mode shapes.

According to Table 4.9’s the second column, the common feature of critical positions is that the end effector is at the top or at the bottom.

The most generalized positions considered to be critical according to the second and third rows of Table 4.9 are shown in Figure 4.4.

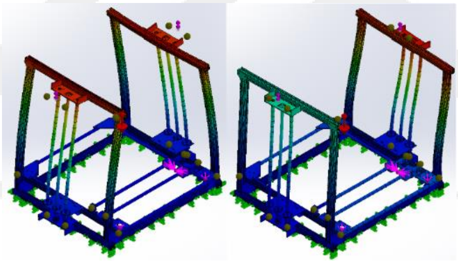

Figure 4.4 The critical mode shapes according to Table 4.8

4.7.3 Performing Impact Hammer Test and Processing the Results

After the chassis is assembled. The chassis was bolted to a rigid surface in accordance with the boundary conditions in the modal analysis. The Impact Hammer Modal Test was performed similar to Schwarz and Richardson's 1999 work by hammering the directions of x and y axis (Figure 4.5). The transmission information obtained during the test was recorded by a computer using a wireless accelerometer. FFT Analysis was performed by using Matlab "Signal Processing" library, then the information obtained was visualized and graphs to be compared with the results obtained from Modal Analysis were obtained. The results of this phase are shown at Table 4.10.

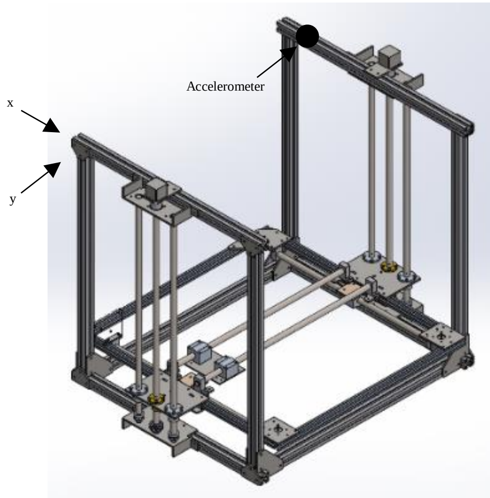

Figure 4.5 Design of Cartesian magnetic flux mapper

Table 4.10 FFT Results of critical positions impact hammer test

Pos. Name	**Impact Direction x**	**Impact Direction y**
ako	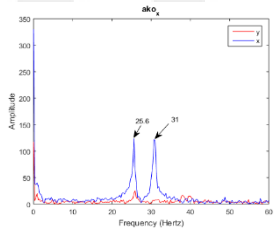	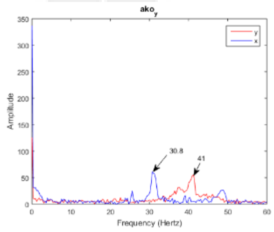
aks	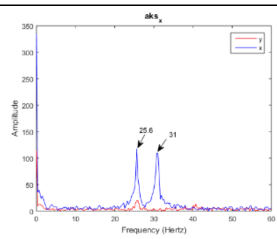	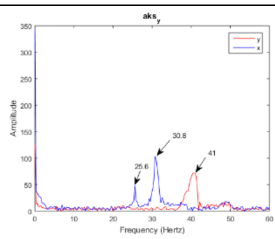
aoo	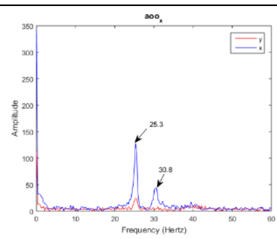	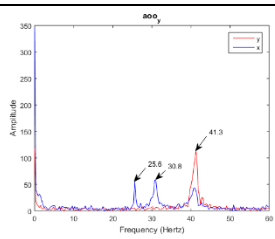

Table 4.10 continues

oko	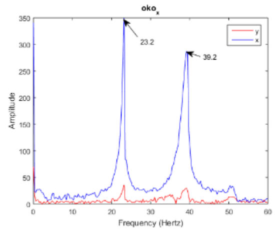	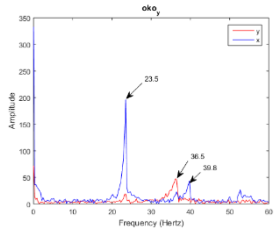
oks	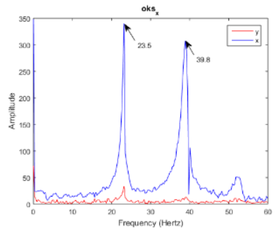	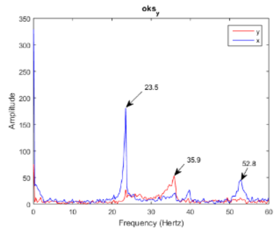
ooo	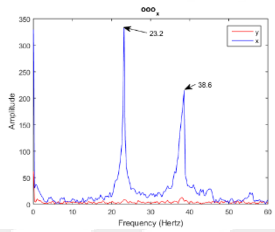	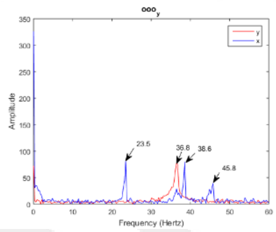
uko	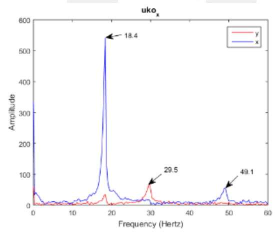	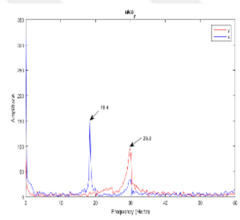
uks	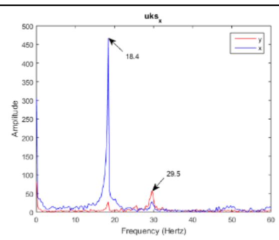	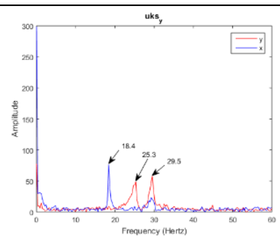

"aos", "oos", "uoo", and "uos" not measured because they show close values according to the information in Table 4.10.

Table 4.11 Summary of impact hammer test

	Impact Direction	**X**		**Y(Hz)**	
ags	**x**	25.6	30.4	-	-
	y	25.9	30.8	41	-
ako	**x**	25.6	31	-	-
	y	30.8	-	41	-
aks	**x**	25.6	31	-	-
	y	25.6	30.8	41	-
aoo	**x**	25.3	30.8	-	-
	y	25.6	30.8	41.3	-
ogs	**x**	22.9	39.5	-	-
	y	22.9	39.5	35.3	-
oko	**x**	23.2	39.2	-	-
	y	23.5	39.8	36.5	-
oks	**x**	23.5	39.8	-	-
	y	23.5	52.8	35.9	-
ooo	**x**	23.2	38.6	-	-
	y	23.4	38.6	36.8	-
ugs	**x**	18.4	-	29.6	-
	y	18.4	-	25	29.5
uko	**x**	18.4	49.1	29.5	-
	y	18.4	-	29.8	-
uks	**x**	18.4	-	29.5	-
	y	18.4	-	25.3	29.5

Comparing of Table 4.10 and Table 4.11 shows us in the world conditions the higher the elevator part, the lower the frequency. Such as reverse pendulum. At the minimum measured frequency to resonate the system you need 18 Hz of vibration or 1104 rpm of motor movement

4.7.4 Performing Movement Test and Processing the Results

While performing this test, the "end effector" was moved for 10mm by the velocity profile given below (Figure 4.6) and specs according to Table 3. And with the wireless accelerometer placed on the “end effector”, the data was recorded on the computer. Matlab "Signal Processing" library FFT analysis was performed. The results were visualized and examined.

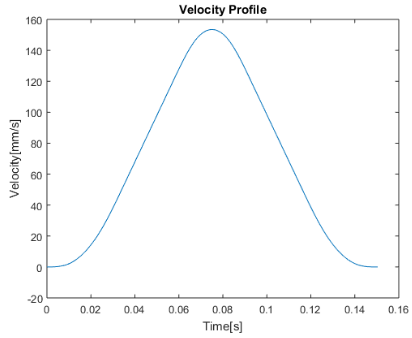

Figure 4.6 Velocity profile of test movement

Table 4.12 Specifications of velocity profile

Variable	**Value**	**Comment**
V_{max}	153.5[mm/s]	Maximum Velocity Value
Acc.	3000[mm/s^2]	Acceleration Value
Disp.	10[mm]	Desired Displacement
T_j	0.025[s]	Jerk Time
T_s	0.025[s]	Snap Time

In these measurements,to name test movements the letter coding used for naming positions was used. In addition, the letter was added to indicate the direction of movement (Figure 4.7).

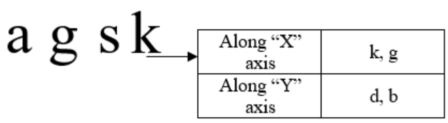

Figure 4.7 Naming methodology of test movements.

In this step, measurements were taken for the positions mentioned in Table 4.11 in accordance with the velocity profile in Figure 4.6 in the x axis and y axis direction. Since it was decided that the positions at the top were critical, the focus was on the data of movements with the initial letter "u".

Table 4.13 The movement test results

<table>
<tr><th><u>Positions</u></th><th><u>Graphs</u></th><th><u>Comments</u></th></tr>
<tr><td>ugsd</td><td>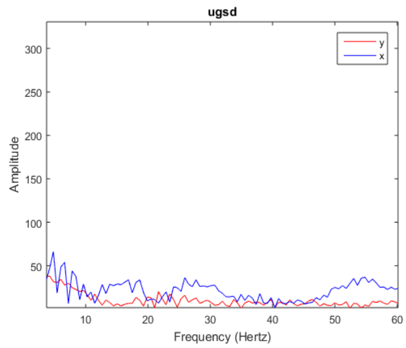
</td><td>There was no significant peak.</td></tr>
<tr><td>ugsk</td><td>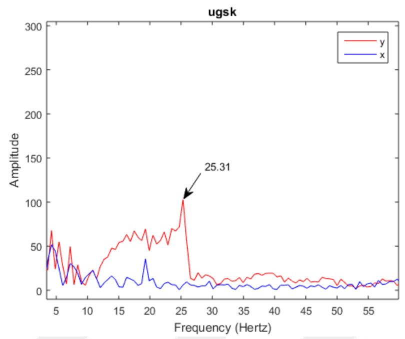
</td><td>A peak at 25.31 Hz was seen along the y axis.</td></tr>
<tr><td>ukod</td><td>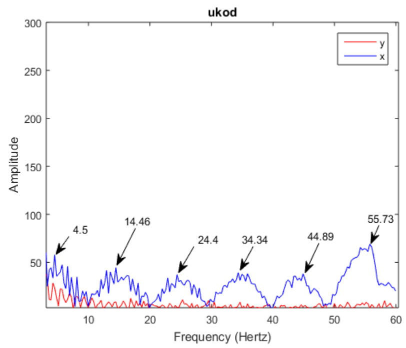
</td><td>Harmonic peaks were observed starting at 4.5 Hz with approximately 10 Hz intervals. It is likely that there is a mechanical gap due to the alignment of the stepper motors in this section.</td></tr>
</table>

Table 4.13 continues

ukog	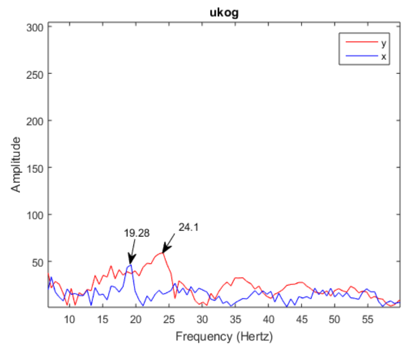	A peak at 24.1 Hz was seen along the y axis. A peak at 19.28 Hz was seen along the x axis.
uksd	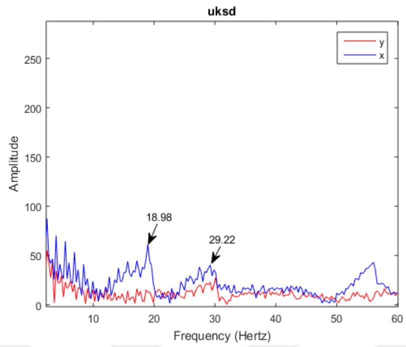	Peaks were seen at 18.98 Hz and 29.22 Hz along the x axis.
uksg	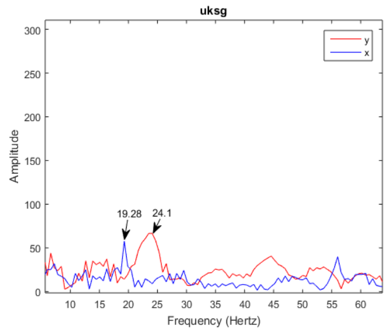	A peak at 24.1 Hz was seen along the y axis. A peak at 19.28 Hz was seen along the x axis.

4.8 Finite Element Model of Test Magnet Circuit

The main purpose of mapping the magnetic field is to measure whether a previously made magnet circuit provides the desired performance and to see if there is a defect in its internal structure.

As a result of the measurements, a model of partial differential equation (PDE) which is close to the expected structure was created. A broken magnet is placed in the model.

With Matlab PDE Modeler tool firstly geometric model has been developed in 2D.

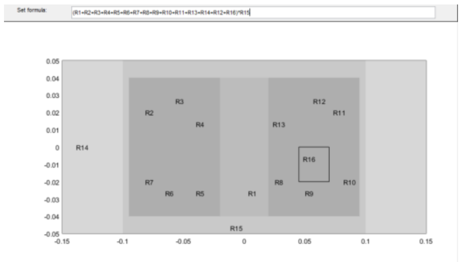

Figure 4.7 2D magnet array model

R14 was environment as air, R1 was metal plate, R2 to R12 and R16 were magnets and R15 was boundary. For model geometry field formula has been set as below equation.

$$(R1 + R2 + R3 + R4 + R5 + R6 + R7 + R8 + R9 + R10 + R11 + R13 + R14 + R12 + R16) * R15 \tag{4.1}$$

The type of application was set as Magnetostatics.

Boundary conditions have been defined as Dirichlet.

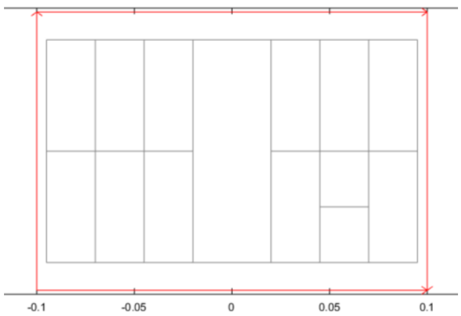

Figure 4.8 Boundary conditions are visualized

As Rao's study ceramic magnets current density has been set to approximately 170000 A/m^2.

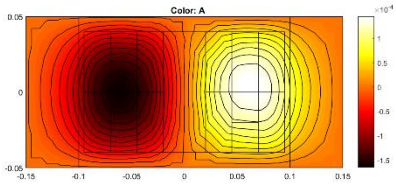

Figure 4.9 Expected visual after magnetic field mapping

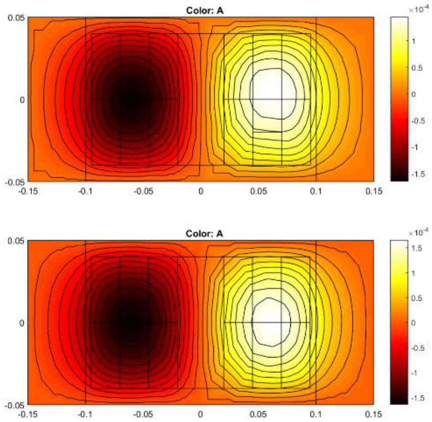

Figure 4.10 Comparison of with regular magnet and broken magnet

As shown in Figure 4.10 the crack on magnet changes negatively magnetic field.

CHAPTER FIVE

RESULTS

CMFM has been assembled and operated due to design conditions. At the end of the assembly, a machine with external dimensions of 930 x 740 x 835 was obtained. And CMFM is approx. 28 kg.

During operation, the "end effector" can travel a volume of 600x 303x 640 mm.

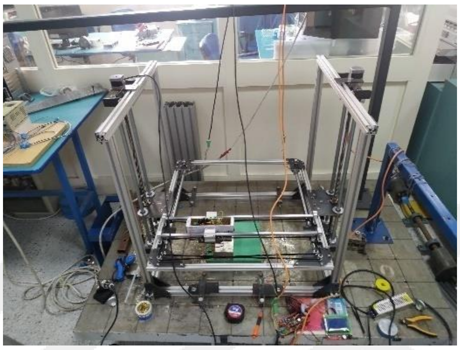

Figure 5.1 CMFM on operation (Personal archive, 2019)

Figure 5.2 The test magnetic circuit with broken magnet (Personal archive, 2019)

A test magnetic circuit has been prepared with a broken magnet. The goal is finding failure inside of magnet.

Figure 5.3 Magnetic circuit (Personal archive, 2019)

To simulate real-world application, the magnetic circuit was sealed with stainless steel by squeezing PU foam into it.

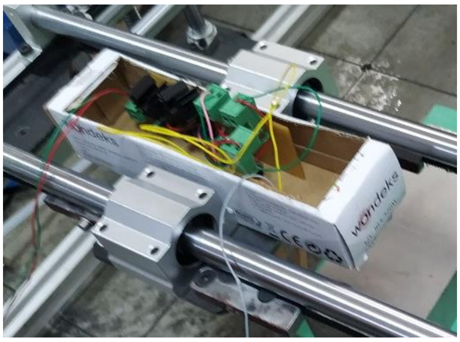

Figure 5.4 Circuit group of sensor instrumentation (Personal archive, 2019)

The amplifier circuit output is tuned to 1 to 4.5 V but at the final the range is 1 to 3.7 V. This error has been compensating on software side.

To Generate toolpath of sensor a fundamental CAM program has been developed in Python Programming Language. Another software was developed to collect sensor data on the computer via the USB port. That software is given in the appendices section.

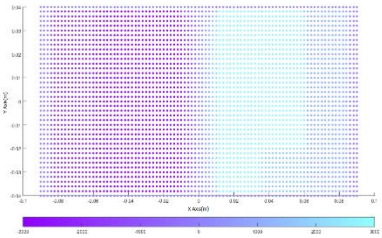

Figure 5.5 Magnetic flux readings of magnetic circuit's surface XY plane

As shown in the Figure 5.5, deterioration of the magnetic flux was caught at the location of the broken magnet.

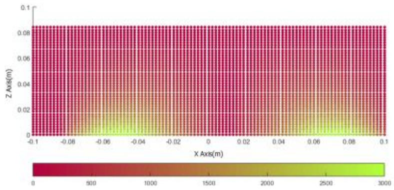

Figure 5.6 Force index of magnetic circuit's middle plane XZ plane

The magnetic circuit can attract M4 nut from 50 mm. According to Figure 5.6 above maximum force index at that distance is approximately 1870. It is suits with Table 1.1 with minor error.

CHAPTER SIX
CONCLUSION

Within the scope of the thesis, a machine is combined in mechanical, electronic and software comprehension in order to capture the performance conditions and errors of a magnetic circuit. Stepper motors for precise positioning, special circuits for driving these motors, and software for instant access to magnetic flux information were used. The mapping of the magnetic field is a new issue of importance. The special feature of CMFM is that it is designed to be portable.

However, in order to be used in the market, it needs to go further. Because the design has been not plugged and run, yet. To reach graphical information and report still needs a lots of post processing. But this method can still be used for quality, performance and integrity control of magnetic circuits. It can be moved by moving to the measurement location. Reporting with a little programming skill can be taken care of.

In the future works, general construction might be mono block, and reporting method could be standardized. And also, electronics are very fragile most of them are design for 3D printers and suits for clean environments.

REFERENCES

20x20 sigma profile, (n.d.). Retrieved August 8, 2019 from http://www.hksaluminyum.com.tr/eng/sigma-profilleri/20x20-sigma-25-5524_620

30x30 sigma profile, (n.d.). Retrieved August 8, 2019 from http://www.hksaluminyum.com.tr/imagesbuyuk/25-5526.jpg

A4988 stepper motor driver, (n.d.). Retrieved August 8, 2019 from https://www.google.com/imgres?imgurl=https%3A%2F%2Fwww.cytron.io%2Fimage%2Fcache%2Fcatalog%2Fproducts%2FSD-A4988%2FSD-A4988-0-1-1-800x800.jpg&imgrefurl=https%3A%2F%2Fwww.cytron.io%2Fp-a4988-stepper-motor-driver-module&tbnid=bzkixWHgtGiZdM&vet=12ahUKEwjamNyWl6_kAhVQgRoKHXy-CRkQMygBegQIARBs..i&docid=UgyeE_jr7HnZjM&w=800&h=800&q=A4988%20Stepper%20Motor%20Driver&safe=active&ved=2ahUKEwjamNyWl6_kAhVQgRoKHXy-CRkQMygBegQIARBs

An industrial magnetic separator, (n.d.). Retrieved August 8, 2019 from https://4.imimg.com/data4/XB/AR/MY-1799742/overband-magnetic-separator-500x500.jpg

Angeles J. (2014). *Fundamentals of robotic mechanical systems* (4th ed.). Switzerland: Springer International Publishing.

Arduino integrated development enviroment (IDE) (n.d.). Retrieved August 8 2019 from https://en.wikipedia.org/wiki/Arduino_IDE

Arduino Mega 2560, (n.d.). Retrieved August 8, 2019 from https://www.amazon.com/ARDUINO-MEGA-2560-REV3-A000067/dp/B0046AMGW0

Arduino Mega 2560 references, (n.d.). Retrieved August 8, 2019 from https://www.arduino.cc/

Coey J.M. (2002). Permanent magnet applications. *Journal Of Magnetism And Magnetic Materials 248*, (3), 441-456.

Core XY schema, (n.d.). Retrieved August 8, 2019 from https://corexy.com/reference.png

Goudsmit magnetics group, (n.d.). Retrieved August 8, 2019 from https://www.goudsmitmagnets.com/en/wiki/88/force-index

GT2 trigger belt, (n.d.). Retrieved August 8, 2019 from https://cdn-shop.adafruit.com/datasheets/gt2tooth.jpg

GT2 trigger pulley, (n.d.). Retrieved August 8, 2019 from https://www.palmar.co.ke/wp-content/uploads/2018/01/GT-Pulley-5mm-500x500.jpg

Hall effect sensor AH49H, (n.d.). Retrieved August 8, 2019 from https://www.diodes.com/assets/Datasheets/AH49H.pdf

Hammer nuts, (n.d.). Retrieved August 8, 2019 from https://static.doguskalip.com.tr/imgsrv/Upload/Category/636601899238255922.png

Hex socket bolt, (n.d.). Retrieved August 8, 2019 from https://d10b75yp86lc36.cloudfront.net/Monotaro3/pi/full/mono47338541-130305-02.jpg

Induction hardened linear shaft, (n.d.). Retrieved August 8, 2019 from https://us.misumi-ec.com/linked/material/mech/TLN1/PHOTO/221006228519_001.jpg?$product_main$

JM1 flex coupling, (n.d.). Retrieved August 8, 2019 from https://cf5.s3.souqcdn.com/item/2018/12/05/42/25/13/43/item_XL_42251343_49c43290caed9.jpg

Karagülle H. & Malgaca L. (2004). Analysis of end point vibrations of a two-link manipulator by integrated CAD/CAE procedures. *Finite Elements in Analysis and Design, 40*, 2049-2061.

LMEF linear ball bearing unit, (n.d.). Retrieved August 8, 2019 from https://www.radikalmuhendislik.com/images/radikal%20muhendislik%20-%20LMEF%20UU%20serisi%20bilyali%20rulman.jpg

Marlin firmware, (n.d.). Retrieved August 8, 2019 from https://www.google.com/imgres?imgurl=http%3A%2F%2Fmarlinfw.org%2Fassets%2Fimages%2Flogo%2Fmarlin%2Fsmall.png&imgrefurl=http%3A%2F%2Fmarlinfw.org%2F&tbnid=LzGSchTCu0QTxM&vet=12ahUKEwiYuMawlq_kAhWNw4UKHUcXCBsQMygAegQIARBM..i&docid=Rzyt1kC6DxCkQM&w=200&h=225&q=Marlin%20Firmware&safe=active&ved=2ahUKEwiYuMawlq_kAhWNw4UKHUcXCBsQMygAegQIARBM

NEMA 17 rpm torque diagram, (n.d.). Retrieved August 8, 2019 from https://www.google.com/imgres?imgurl=https%3A%2F%2Fd2nlp3g45tnwoj.cloudfront.net%2Fstaticpic%2Fimages%2FMS17HD2P4040.png&imgrefurl=https%3A%2F%2Fwww.moonsindustries.com%2Fseries%2Fnema-17-standard-hybrid-stepper-motors-b020105&tbnid=n-01vr4eI3A2PM&vet=12ahUKEwi5_vCul6_kAhWQwYUKHZGwBxMQMygBegQIARBH..i&docid=l5fwl3NSOU4sHM&w=663&h=726&q=NEMA%2017%20rpm%20torque%20diagram&safe=active&ved=2ahUKEwi5_vCul6_kAhWQwYUKHZGwBxMQMygBegQIARBH

NEMA 17 stepper motor, (n.d.) Retrieved August 8, 2019 from https://www.google.com/imgres?imgurl=https%3A%2F%2Faus3d.com.au%2Fimage%2Fcache%2Fcatalog%2Fproducts%2Fstepper%2FgenericStepper2-800x800.jpg&imgrefurl=https%3A%2F%2Faus3d.com.au%2Fnema17-stepper-34mm&tbnid=yuiOu9DWjRoYnM&vet=12ahUKEwjorMqgl6_kAhVL3hoKHRdVD5cQMygDegQIARB5..i&docid=dUU9BhIvVfsOlM&w=800&h=800&q=NEMA%2017%20Stepper%20Motor&safe=active&ved=2ahUKEwjorMqgl6_kAhVL3hoKHRdVD5cQMygDegQIARB5

Oberteuffer J. (1973), High gradient magnetic separation, *IEEE Transactions on Magnetics, 40*, 303-306.

Power supply 12V 200W, (n.d.). Retrieved August 8, 2019 from https://www.makerlab-electronics.com/product/12v-switching-power-supply-200w/

Rao S. & Prasad P. (2012). Finite Element Method Using PDETOOL of Matlab for Hybrid Stepper Motor Design ,*TELKOMNIKA, 10*, 4, 741-748

RepRap 1.4 shield, (n.d.). Retrieved August 8, 2019 from https://www.miniinthebox.com/tr/p/3d-yazici-modulu-karti-cam-fiber-harici-guc-kaynagi-arduino_p7014910.html

RepRap 12864 LCD smart display, (n.d.). Retrieved August 8, 2019 from https://www.amazon.co.uk/Redrex-Graphic-Display-Controller-Printer/dp/B01LO20XGS

RepRap project, (n.d.). Retrieved August 8, 2019 from https://en.wikipedia.org/wiki/RepRap_project

SCE linear bearing unit, (n.d.). Retrieved August 8, 2019 from https://www.tradebearings.com/product-photo/archive/6dRjkf99FJuweCs8ZHT/sce20-linear-motion-ball-bearing-slide-unit-20x54x41mm.jpg

SHF linear shaft support, (n.d.). Retrieved August 8, 2019 from https://www.cnballscrew.com/uploads/201715352/shf-linear-shaft-support48304498212.jpg

Shoulder bolt, (n.d.). Retrieved August 8, 2019 from https://cdn11.bigcommerce.com/s-hlsk6yq0/images/stencil/1280x1280/products/301774/1267079/item-shoulder-screw-pellet-pln__12180.1539211830.jpg?c=2

SK linear shaft support, (n.d.). Retrieved August 8, 2019 from https://www.diyelectronics.co.za/store/3052-large_default/sk16-linear-shaft-support.jpg

Svoboda J.& Fujita T. (2003). Recent developments in magnetic methods of material separation. *Minerals Engineering,16,* 9, 785-792.

Texas Ins.single-supply op amp design techniques (2001) Retrieved August 8, 2019 from http://www.ti.com/lit/an/sloa030a/sloa030a.pdf

The logo of Marlin firmware, (n.d.). Retrieved August 8, 2019 from http://marlinfw.org/

TL072 Op Amp Schema, (n.d.). Retrieved August 8, 2019 from http://vakits.com/tl072-smt-dual-jfet-op-amp

Trapezoidal screw and variations of nuts, (n.d.) Retrieved August 8, 2019 from https://www.amazon.com/400mm-Screw-Thread-Copper-Printer/dp/B00YPV1LMQ

Trapezoidal screws and nuts, (n.d.). Retrieved August 8, 2019 from https://www.abssac.co.uk/uploads/site/docbooks/4_cover_PowerScrewsTrapezoidal.jpg

UFL bearing unit, (n.d.). Retrieved August 8, 2019 from https://i.ebayimg.com/images/g/3HsAAOSwr8tblv5O/s-l300.jpg

APPENDICES

Appendix 1: CAM Software

```
from datetime import datetime
import math



now=datetime.now()
dt_string = now.strftime("%d%m%Y%H%M%S")

incX = 10
incY = 10
incZ = 10

coorInit = [0, 0, 0]#Initial coordinates in mm[X,Y,Z]
coorLast = [210, 100, 30]#Lasrt coordinates in mm[X,Y,Z]
def stepFunc(initial, last, inc):
  return math.ceil((last-initial)/inc)

def gCodeGen(list):
    strt = "G1 X"+str(list[0])+" Y"+str(list[1])+" Z"+str(list[2])+" F3800\nM105\n G4 P50\n"
    return strt

temp=[stepFunc(coorInit[0], coorLast[0], incX),stepFunc(coorInit[1], coorLast[1], incY),stepFunc(coorInit[2], coorLast[2], incZ)]
coorUpLimit = [coorInit[0]+incX*temp[0], coorInit[1]+incY*temp[1],coorInit[2]+incY*temp[2]]
coorCurrent = [coorInit[0],coorInit[1],coorInit[2]]
coors=[]
```

```
path ='C:/Users/Ufuk AKOĞUZ/Desktop/gcode/' + dt_string+'.gcode'
with open(path,'w',newline='')as f:
    f.write("G28\nG90\n")
    for z in range(temp[2] + 1):
        for y in range(temp[1] + 1):
            if y % 2 == 0:
                for x in range(temp[0]):
                    # print(coorCurrent)
                    f.write(gCodeGen([coorCurrent[0], coorCurrent[1], coorCurrent[2]]))
                    coorCurrent[0] = coorCurrent[0] + incX
                # print(coorCurrent)
                f.write(gCodeGen([coorCurrent[0], coorCurrent[1], coorCurrent[2]]))
                coorCurrent[1] = coorCurrent[1] + incY
            if y % 2 == 1:
                for x in range(temp[0]):
                    # print(coorCurrent)
                    f.write(gCodeGen([coorCurrent[0], coorCurrent[1], coorCurrent[2]]))
                    coorCurrent[0] = coorCurrent[0] - incX
                # print(coorCurrent)
                f.write(gCodeGen([coorCurrent[0], coorCurrent[1], coorCurrent[2]]))
                coorCurrent[1] = coorCurrent[1] + incY
        coorCurrent = [coorInit[0], coorInit[1], coorCurrent[2] + incZ]
    f.write("M84\n")
```

Appendix 2: USB Connection Software

```
import serial
import math
import time
import csv
from datetime import datetime

ser = serial.Serial('COM5', baudrate=250000,  timeout=1)
whileBool = True
homming = True

incX = 10
incY = 10
incZ = 10

coorInit = [0, 0, 0]#Initial coordinates in mm[X,Y,Z]
coorLast = [210, 100, 30]#Lasrt coordinates in mm[X,Y,Z]
def sendmes(sttr, status, seri):
   if "ok" in status:
      seri.write(sttr)
def stepFunc(initial, last, inc):
   return math.ceil((last-initial)/inc)

def commandGen(list):
   strt = "G1X"+str(list[0])+"Y"+str(list[1])+"Z"+str(list[2])+"F3800\nM105\n"
   return strt.encode('utf8')

#coordinate process
temp=[stepFunc(coorInit[0], coorLast[0], incX),stepFunc(coorInit[1], coorLast[1], incY),stepFunc(coorInit[2], coorLast[2], incZ)]
coorUpLimit = [coorInit[0]+incX*temp[0], coorInit[1]+incY*temp[1],coorInit[2]+incY*temp[2]]
```

```
coorCurrent = [coorInit[0],coorInit[1],coorInit[2]]
coors=[]

for z in range(temp[2]+1):
    for y in range(temp[1]+1):
        if y % 2 == 0:
            for x in range(temp[0]):
                #print(coorCurrent)
                coors.append([coorCurrent[0],coorCurrent[1],coorCurrent[2]])
                coorCurrent[0] = coorCurrent[0] + incX
            #print(coorCurrent)
            coors.append([coorCurrent[0], coorCurrent[1], coorCurrent[2]])
            coorCurrent[1] = coorCurrent[1]+incY
        if y% 2 == 1:
            for x in range(temp[0]):
                #print(coorCurrent)
                coors.append([coorCurrent[0], coorCurrent[1], coorCurrent[2]])
                coorCurrent[0] = coorCurrent[0] - incX
            #print(coorCurrent)
            coors.append([coorCurrent[0], coorCurrent[1], coorCurrent[2]])
            coorCurrent[1] = coorCurrent[1]+incY
    coorCurrent=[coorInit[0],coorInit[1],coorCurrent[2]+incZ]
#print(coors)

counter=0
now=datetime.now()
dt_string = now.strftime("%d%m%Y%H%M%S")

print(dt_string)
path ='C:/Users/Ufuk AKOĞUZ/Desktop/csv/' + dt_string+'.csv'

with open(path,'w',newline='')as f:
```

```
    thewriter = csv.writer(f)

    while whileBool:
        line = ser.readline()
        strLine = line.decode('utf8')
        #print(strLine)
        if "echo" in strLine:
            time.sleep(0.1)
            print(strLine)

        if "ok" in strLine:
            #if counter == 0 and homming:
                #sendmes(b'G28\n', strLine, ser)#homming and absolute coordinates
                #time.sleep(5)
                #sendmes(b'G90\n', strLine, ser)
                #sendmes(b'M105\n', strLine, ser)
                #homming=False

            if counter != len(coors) :
                if "T" in strLine and "echo" not in strLine:
                    q=strLine.split(" ")
                    print(strLine)
                    t=q[1].split(":")
                    #sendmes(commandGen(coors[counter]), strLine, ser)
                    time.sleep(0.1)
                    #sendmes(b'M105\n', strLine, ser)
                    thewriter.writerow([coors[counter][0], coors[counter][1],
coors[counter][2],t[1]])
                    print(commandGen(coors[counter]))
                    print(counter)
                    counter = counter + 1
```

```
        #time.sleep(1)
        #delay = (temp[0]+1)*(temp[1]+1)+1
        #if counter%delay==0:
            #time.sleep(10)
        if counter%100 == 0:
            sendmes(b'G92\nG90\n', strLine, ser)
if "Done printing file" in strLine:
    whileBool = False
```